PLOS ONE

RESEARCH ARTICLE

Analysis of ferrite nanoparticles in the flow of ferromagnetic nanofluid

Noor Muhammad[1]*, Sohail Nadeem[1], M. T. Mustafa[2]

1 Department of Mathematics, Quaid-I-Azam University 45320, Islamabad 44000, Pakistan, **2** Department of Mathematics, Statistics and Physics, Qatar University, Doha 2713, Qatar

* noor@math.qau.edu.pk

OPEN ACCESS

Citation: Muhammad N, Nadeem S, Mustafa MT (2018) Analysis of ferrite nanoparticles in the flow of ferromagnetic nanofluid. PLoS ONE 13(1): e0188460. https://doi.org/10.1371/journal.pone.0188460

Editor: Bing Xu, Brandeis University, UNITED STATES

Received: April 26, 2017

Accepted: November 7, 2017

Published: January 10, 2018

Data Availability Statement: All relevant data are within the paper.

Funding: Authors would like to acknowledge and express their gratitude to the Qatar University Doha 2713, Qatar, for providing the financial support to publish this article.

Competing interests: The authors have declared that no competing interests exist.

Abstract

Theoretical analysis has been carried out to establish the heat transport phenomenon of six different ferromagnetic $MnZnFe_2O_4$—$C_2H_6O_2$ (manganese zinc ferrite-ethylene glycol), $NiZnFe_2O_4$—$C_2H_6O_2$ (Nickel zinc ferrite-ethylene glycol), Fe_2O_4—$C_2H_6O_2$ (magnetite ferrite-ethylene glycol), $NiZnFe_2O_4$—H_2O (Nickel zinc ferrite-water), $MnZnFe_2O_4$—H_2O (manganese zinc ferrite-water), and Fe_2O_4—H_2O (magnetite ferrite-water) nanofluids containing manganese zinc ferrite, Nickel zinc ferrite, and magnetite ferrite nanoparticles dispersed in a base fluid of ethylene glycol and water mixture. The performance of convective heat transfer is elevated in boundary layer flow region via nanoparticles. Magnetic dipole in presence of ferrites nanoparticles plays a vital role in controlling the thermal and momentum boundary layers. In perspective of this, the impacts of magnetic dipole on the nano boundary layer, steady, and laminar flow of incompressible ferromagnetic nanofluids are analyzed in the present study. Flow is caused by linear stretching of the surface. Fourier's law of heat conduction is used in the evaluation of heat flux. Impacts of emerging parameters on the magneto—thermomechanical coupling are analyzed numerically. Further, it is evident that Newtonian heating has increasing behavior on the rate of heat transfer in the boundary layer. Comparison with available results for specific cases show an excellent agreement.

1 Introduction

Heat transfer enhancement in a two-phase fluid flow has been scrutinized for many years. In heat transfer equipment liquids are frequently utilized as heat transporter. Research on nanofluid flow depicts that by adding ferrite nanoparticles in the fluid, the heat transfer coefficient can be enhanced. The resulting increase in the heat transfer, in addition to the possible rise in thermal conductivity, was mainly because of the reduced thickness of the thermal boundary layer. It is very probable that motion of ferrite nanoparticles in the fluid will enhance thermal conductivity and heat transfer. Examples of important uses of heat transfer liquids include hydronic and cooling heating systems in buildings, vehicular and avionics cooling systems in industry, chemical, foods, and other processing plants. In all the mentioned applications, the

thermal conductivity of heat transfer liquids play a vital role in the construction of energy-efficient heat transport equipment. It is suggested that nano-meter metallic particles can be suspended in heat transfer fluids such as ethylene glycol, water or engine oil to a new class of fluid with high thermal conductivity, the resulting fluid is termed as nanofluid [1]. Nanofluid displays better quality when compared with fluids containing micrometer-sized particles and conventional heat transfer liquids. Since heat transfer results on the surface of the particle, it is necessary to use nanoparticle with large surface area. Nanoparticles have sufficiently large surface area as compare to micrometer-sized particles, and therefore nanofluids have extensive potential for application [2–10] in heat transfer.

Ferrofluids are colloidal liquids made of ferrimagnetic or ferromagnetic ferrite nanoparticles slanged in an electrically non-conducting carrier fluid. In present study, the considered ferrite nanoparticles are $MnZnFe_2O_4$ (manganese zinc ferrite), Fe_2O_4 (magnetite ferrite), and $NiZnFe_2O_4$ (nickel zinc ferrite) [11, 12] crystallizes in the normal spinal structure. The carrier fluid is taken to be water (H_2O) and ethylene glycol ($C_2H_6O_2$). In ferromagnetic nanofluids hyperthermia, ferrites nanoparticles of various types like $MnZnFe_2O_4$, Fe_2O_4, and $NiZnFe_2O_4$ or even of hematite are infused in tumor and afterward subjected under a high frequency magnetic field. These ferrite nanoparticles produce heat that regularly enhances tumor temperature, which can kill cancer cell [13] A well-tempered of these ferrites are, therefore, characterized by containing the iron atoms situated at the origins of octahedra of oxygen atoms and zinc atoms originated in tetrahedra of oxygen atoms. Characteristically, the normal spinels are paramagnetic and the inverted spinels are ferromagnetic at the room temperature. Further, at low temperature zinc ferrites are behave like antiferromagnetic. Ferrofluids do not hold magnetization in the absence of a magnetic dipole and are classified into superparamagnets. A remarkable feature of the ferromagnetic nanofluids is the reliance of magnetization on the temperature and this thermomagnetization coupling makes ferromagnetic nanofluids more applicable in various practical applications [14–17]. Ferrofluids can be used to capture magnetic domain structures on the surface of ferrofluids in presence of magnetic dipole utilizing a procedure introduced by Mee [18]. The flow of a ferrofluid under the impact of magnetic field and thermal gradients are explored by Neuringer [19]. Nadeem *et al.* [20] depicted the influence of a magnetic dipole with porous medium in the flow of a ferrofluid. Anderson and Valnes [21] analyzed the effects of a magnetic field produced by magnetic dipole over a stretched sheet (shear driven motion) and concluded that the magnetic field is responsible for slow downing the motion of fluid. Zeeshan and Majeed demonstrated the influence of the magnetic dipole and suction/injection in a Jeffrey fluid flow over a stretchable surface [22]. Heat transfer analysis in a ferromagnetic fluid flow over a stretching surface is exposed by Majeed *et al.* [23]. Some applications relevant to the flow of liquids may be found in [24–35].

The purpose of the article is to exhibit theoretically the practicability of the concept of ferromagnetic nanoparticles with Fe_2O_4 (magnetite ferrite), $NiZnFe_2O_4$ (Nickel zinc ferrite), and $MnZnFe_2O_4$ (manganese zinc ferrite) as ferrites nanoparticles and $C_2H_6O_2$ (ethylene glycol) and H_2O (water) as base fluid. The present analysis concentrates on depicting the heat transport phenomenon in the flow of ferromagnetic nanofluids. A comparison has been made for different ferrites nanoparticles in the analysis of axial velocity, temperature field, wall shear stress and heat transfer rate. The constitutive equations for velocity and temperature are taken under the boundary layer assumptions. In the wake of utilizing appropriate similarity variables, the final form of boundary value problem is clarified numerically with the help of BVPh2—midpoint method and analytically with optimal homotopy analysis method. The physical emerging parameters are portrayed through tables and graphs.

2 Ferrohydrodynamic and thermal energy equations

2.1 Flow analysis

Consider an electrically non—conducting, steady, an incompressible and laminar viscous boundary layer flow of a ferromagnetic $MnZnFe_2O_4$—$C_2H_6O_2$ (manganese zinc ferrite-ethylene glycol), $NiZnFe_2O_4$—$C_2H_6O_2$ (Nickel zinc ferrite-ethylene glycol), Fe_2O_4—$C_2H_6O_2$ (magnetite ferrite-ethylene glycol), $NiZnFe_2O_4$—H_2O (Nickel zinc ferrite-water), $MnZnFe_2O_4$—H_2O (manganese zinc ferrite-water), and Fe_2O_4—H_2O (magnetite ferrite-water) nanofluids along a continuously stretching surface. The effect of the magnetic dipole is taken in such a way that its center exactly lies on the x—axis. The nanofluid flow is caused due to the stretching of the sheet. The velocity of the stretching sheet is $U_w = Sx$ (S is a dimensionless constant) and $T = T_w$ and $T = T_\infty$ symbolizes the respective temperature at the stretching sheet and ambient fluid. The magnetic field points of magnetic dipole are applied in positive x—direction. To make ferrofluid saturate, the magnetic dipole improve the magnetic field of significant strength. The geometry for the flow evaluation is shown in Fig 1. The fluid above Curie temperature T_c is not capable of being magnetized. It is assumed that the Curie temperature is greater than the temperature at stretching sheet, instead, the temperature $T = T_\infty$ is supposed to be temperature of the fluid away from the surface, where $T_w < T_\infty < T_c$. It is presumed that the nanoparticles and base fluids are in thermal equilibrium and occurs no slip between them. The thermophysical properties of the nanofluids $MnZnFe_2O_4$—$C_2H_6O_2$, $NiZnFe_2O_4$—$C_2H_6O_2$, and Fe_2O_4—$C_2H_6O_2$ are taken as in Table 1. Considering the above assumptions into account, applying the boundary layer approximation $O(u) = O(x) = O(1)$ and $O(v) = O(y) = O(\delta)$, the boundary layer equations in a ferrohydrodynamic and thermal energy

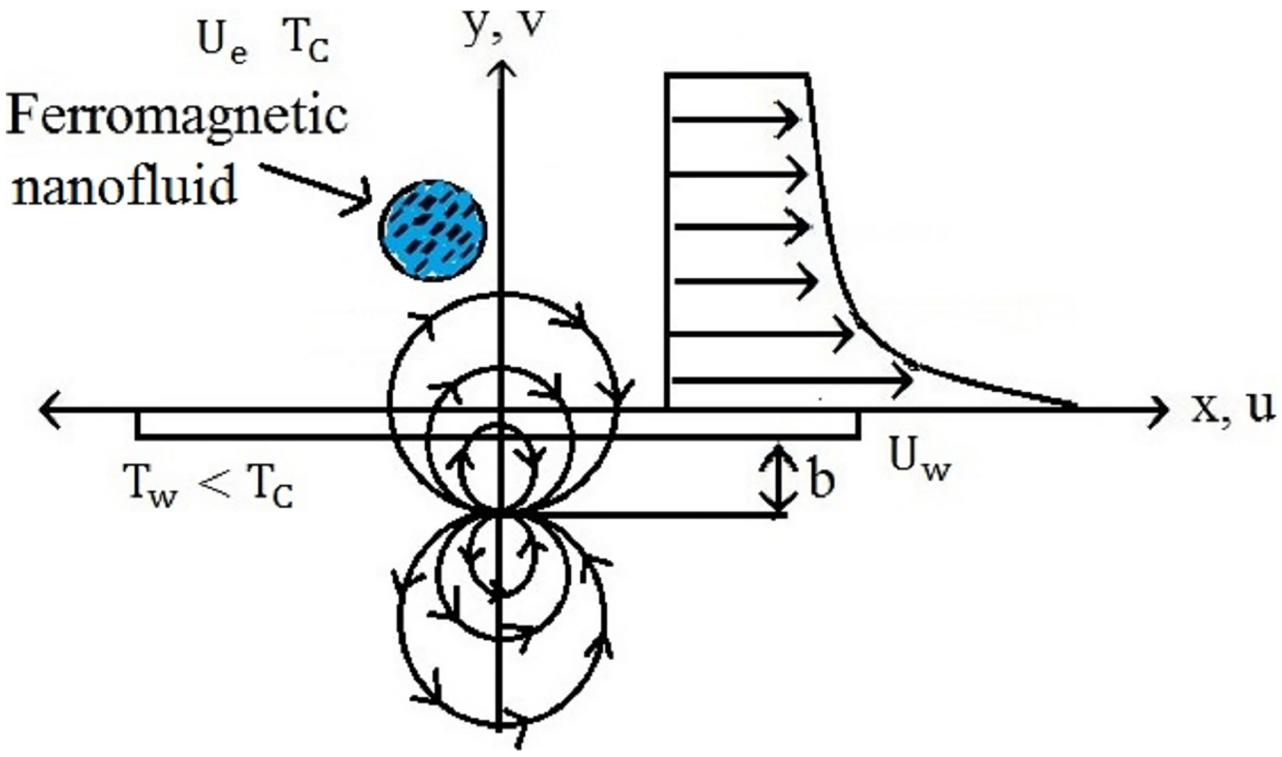

Fig 1. Geometry of the flow problem.

https://doi.org/10.1371/journal.pone.0188460.g001

Table 1. Thermo-physical properties of ethylene glycol, water, manganese zinc ferrite, nickel zinc ferrite, and magnetite ferrite.

	ρ(kg/m^3)	C_p(J/kgK)	k(W/mK)	Pr
Ethylene glycol($C_2H_6O_2$)	1116.6	2382	0.249	204
Water(H_2O)	998.3	4182	0.60	6.96
Nickel zinc ferrite($NiZnFe_2O_4$)	4800	710	6.3	—
Manganese zinc ferrite($MnZnFe_2O_4$)	4700	1050	3.9	—
Magnetite ferrite(Fe_2O_4)	5180	670	9.7	—

https://doi.org/10.1371/journal.pone.0188460.t001

equations are

$$\frac{\partial u}{\partial x}+\frac{\partial v}{\partial y}=0, \tag{1}$$

$$\rho_{nf}\left(u\frac{\partial u}{\partial x}+v\frac{\partial u}{\partial y}\right)=-\frac{\partial p}{\partial x}+\mu_0 M\frac{\partial H}{\partial x}+\mu_{nf}\frac{\partial^2 u}{\partial y^2}-\frac{\upsilon_{nf}\epsilon}{K_1}u, \tag{2}$$

$$(\rho c_p)_{nf}\left(u\frac{\partial T}{\partial x}+v\frac{\partial T}{\partial y}\right)+\left(u\frac{\partial H}{\partial x}+v\frac{\partial H}{\partial y}\right)\mu_0 T\frac{\partial M}{\partial T}=k_{nf}\frac{\partial^2 T}{\partial y^2}, \tag{3}$$

where (u, v) identify the respective components of velocity along (x, y) directions, μ_0 signify the magnetic permeability, P designate pressure, μ_{nf} exemplify the dynamic viscosity of nanofluid, ρ_{nf} indicate nanofluid density, υ_{nf} specify the kinematic viscosity of nanofluid, K_1 and ϵ are the respective permeability and porosity of porous medium, $(\rho c_p)_{nf}$ display the specific heat, T delegate the temperature, k_{nf} identify thermal conductivity of the nanofluid, H communicate the magnetic field, and M exemplify the magnetization.

The admissible boundary conditions for the boundary value problem are assumed to be of the form

$$\begin{aligned} &u|_{y=0}=U_w=Sx,\ v|_{y=0}=0,\ \left.\frac{\partial T}{\partial y}\right|_{y=0}=-h_c T,\ , \\ &u|_{y\to\infty}\to 0,\ T|_{y\to\infty}\to T_\infty=T_c. \end{aligned} \tag{4}$$

In above Eq 4, U_w exemplify the stretching velocity, the temperature condition recommended at $y = 0$ speaks to the Newtonian heating effects, h_c signify heat transfer coefficient, and $y\to\infty$ describes the Curie temperature T_c at the boundaries, T_∞ signify temperature of ambient fluid.

2.2 Thermo-physical properties of $MnZnFe_2O_4$-$C_2H_6O_2$, $NiZnFe_2O_4$-$C_2H_6O_2$, Fe_2O_4-$C_2H_6O_2$, $MnZnFe_2O_4$-H_2O, $NiZnFe_2O_4$-H_2, and Fe_2O_4-H_2O nanofluids

The dynamic viscosity μ_{nf}, the effective dynamic density ρ_{nf}, the specific heat or heat capacitance $(\rho c_p)_{nf}$, and the thermal conductivity k_{nf} of the nanofluid are given by

$$\begin{aligned} &\rho_{nf}=(1-\varphi)\rho_f+\varphi\rho_s,\ \ \frac{\mu_{nf}}{\mu_f}=\frac{1}{(1-\varphi)^{2.5}}, \\ &(\rho C_p)_{nf}=(1-\varphi)(\rho C_p)_f+\varphi(\rho C_p)_s, \\ &\frac{k_{nf}}{k_f}=\frac{(k_s+2k_f)-2\varphi(k_f-k_s)}{(k_s+2k_f)+\varphi(k_f-k_s)}. \end{aligned} \tag{5}$$

Eq 5 is the general relationship used to calculate the density ρ_{nf}, dynamic viscosity μ_{nf}, specific heat $(\rho C_p)_{nf}$, and thermal conductivity k_{nf} for nanofluids. Where k_s and k_f are the respective thermal conductivities of the base fluid and nanoparticle, and φ is the solid volume fraction of nanofluid, ρ_s and ρ_f are the respective densities of the nano-particle and base fluid. The thermo-physical properties of of the present analysis are listed in Table 1.

2.3 Magnetic dipole

The flow of ferrofluid induced by stretching sheet is influenced by the magnetic field due to the magnetic dipole. Magnetic scalar potential δ^* portray the region of a magnetic dipole, which is defined as

$$\delta^* = \frac{\gamma_1}{2\pi}\frac{x}{x^2 + (y+b)^2}, \tag{6}$$

here γ_1 symbolize the strength of magnetic field at the source and b is the distance from the center of magnetic field to x-axis. The components for the magnetic field (H) are

$$H_x = -\frac{\partial \delta^*}{\partial x} = \frac{\gamma_1}{2\pi}\frac{x^2 - (y+b)^2}{(x^2 + (y+b)^2)^2}, \tag{7}$$

$$H_y = -\frac{\partial \delta^*}{\partial y} = \frac{\gamma_1}{2\pi}\frac{2x(y+c)}{(x^2 + (y+c)^2)^2}. \tag{8}$$

Since the magnetic body force is proportional to the gradient of the magnitude of H, we obtain

$$H = \sqrt{\left(\frac{\partial \delta^*}{\partial x}\right)^2 + \left(\frac{\partial \delta^*}{\partial y}\right)^2}. \tag{9}$$

Making use of Eqs 6 and 7 in Eq 8, we get the resulting equations, after reached out in powers of x and held terms up to organize x^2,

$$\frac{\partial H}{\partial x} = -\frac{\gamma_1}{2\pi}\frac{2x}{(y+b)^4}, \tag{10}$$

$$\frac{\partial H}{\partial y} = \frac{\gamma_1}{2\pi}\left(-\frac{2}{(y+b)^3} + \frac{4x^2}{(y+b)^5}\right). \tag{11}$$

The influence of magnetization M with temperature T is defined by the linear expression below,

$$M = K_2(T - T_\infty), \tag{12}$$

here K_2 identifies the pyromagnetic coefficient. The geometry of a heated ferrofluid appears in Fig 1. Here the round lines exhibits the magnetic field.

3 Solution procedure

Here we introduce the nondimensional variables as exposed by Andersson [9]

$$\psi(\eta,\xi)=\left(\frac{\mu_f}{\rho_f}\right)\eta f(\xi),\qquad \theta(\eta,\xi)\equiv\frac{T_c-T}{T_c-T_w}=\theta_1(\xi)+\eta^2\theta_2(\xi), \tag{13}$$

in which μ_f represents the dynamic viscosity, $\theta_1(\eta,\xi)$ and $\theta_2(\eta,\xi)$ displays the dimensionless temperature, the corresponding non—dimensional coordinates are

$$\xi=y\left(\frac{\rho_f S}{\mu_f}\right)^{1/2},\quad \eta=x\left(\frac{\rho_f S}{\mu_f}\right)^{1/2}. \tag{14}$$

The stream function are delineated in such a way that the continuity equation is directly satisfied, the comparable velocity components u and v are defined as follow

$$u=\frac{\partial\psi}{\partial y}=Sxf'(\xi),\quad v=-\frac{\partial\psi}{\partial x}=-(S\upsilon_f)^{1/2}f(\xi), \tag{15}$$

here prime denotes differentiation with respect to ξ. Making use of the dimensionless variables defined in Eqs (16–18), the Eqs (2) and (3) along with admissible boundary conditions are given in Eq (4) reduces to the following form of coupled equations and corresponding boundary conditions

$$\frac{1}{(1-\varphi)^{2.5}(1-\varphi+\varphi\frac{\rho_s}{\rho_f})}f'''-f'^2+ff''-\frac{2\beta\theta_1}{(1-\varphi+\varphi\frac{\rho_s}{\rho_f})(\xi+\gamma)^4}-\frac{P_m}{(1-\varphi+\varphi\frac{\rho_s}{\rho_f})}f'=0, \tag{16}$$

$$\frac{k_{nf}/k_f}{(1-\varphi+\varphi\frac{(\rho C_p)_s}{(\rho C_p)_f})}\theta_1''+\Pr(f\theta_1'-2f'\theta_1)+\frac{2\lambda\beta f(\theta_1-\varepsilon)}{(\xi+\gamma)^3}-4\lambda f'^2=0, \tag{17}$$

$$\frac{k_{nf}/k_f}{(1-\varphi+\varphi\frac{(\rho C_p)_s}{(\rho C_p)_f})}\theta_2''-\Pr(4f'\theta_2-f\theta_2')+\frac{2\lambda\beta f\theta_2}{(\xi+\gamma)^3} -\lambda\beta(\theta_1-\varepsilon)\left(\frac{2f'}{(\xi+\gamma)^4}+\frac{4f}{(\xi+\gamma)^5}\right)-\lambda f''^2=0, \tag{18}$$

$$f(\xi)=0,\ f'(\xi)=1,\ \theta_1'(\xi)=-\lambda_1(1+\theta_1(0)),\ \theta_2(\xi)=0,\quad \text{at } \xi=0, \tag{19}$$

$$f'(\xi)\to 0,\ \theta_1(\xi)\to 0,\ \theta_2(\xi)\to 0,\quad \text{when } \xi\to\infty. \tag{20}$$

In above system of nonlinear equations, the parameters λ (viscous dissipation), λ_1 (the conjugate parameter of Newtonian heating), β (ferrohydrodynamic interaction), P_m (porosity

Table 2. Shows the average residual square errors (Δ_m^t).

$\frac{values\rightarrow}{order\downarrow}$	$\hbar_f$	$\hbar_{\theta_1}$	$\hbar_{\theta_2}$	Δ_m^t
4	−0.40025	−0.42903	−0.97231	0.009324
6	−0.44380	−0.49902	−0.98331	2.5489×10^{-4}
8	−0.54992	−0.49930	−0.99005	1.09211×10^{-10}
10	−0.60321	−0.54173	−0.92152	3.62310×10^{-15}
12	−0.76119	−0.76497	−1.10921	7.16290×10^{-21}

https://doi.org/10.1371/journal.pone.0188460.t002

Table 3. Shows individual residual square errors for Δ_m^f, $\Delta_m^{\theta_1}$, and $\Delta_m^{\theta_2}$.

$\frac{values\rightarrow}{order\downarrow}$	$\hbar_f = -0.76119$	$\hbar_{\theta_1} = -0.76497$	$\hbar_{\theta_2} = -1.10921$
	Δ_m^f	$\Delta_m^{\theta_1}$	$\Delta_m^{\theta_2}$
8	2.54891×10^{-20}	3.44370×10^{-10}	9.54570×10^{-10}
10	6.43670×10^{-22}	1.45219×10^{-16}	0.64881×10^{-14}
12	0.32671×10^{-25}	8.33670×10^{-20}	6.45672×10^{-18}
20	2.34589×10^{-26}	1.54891×10^{-25}	2.43370×10^{-23}

https://doi.org/10.1371/journal.pone.0188460.t003

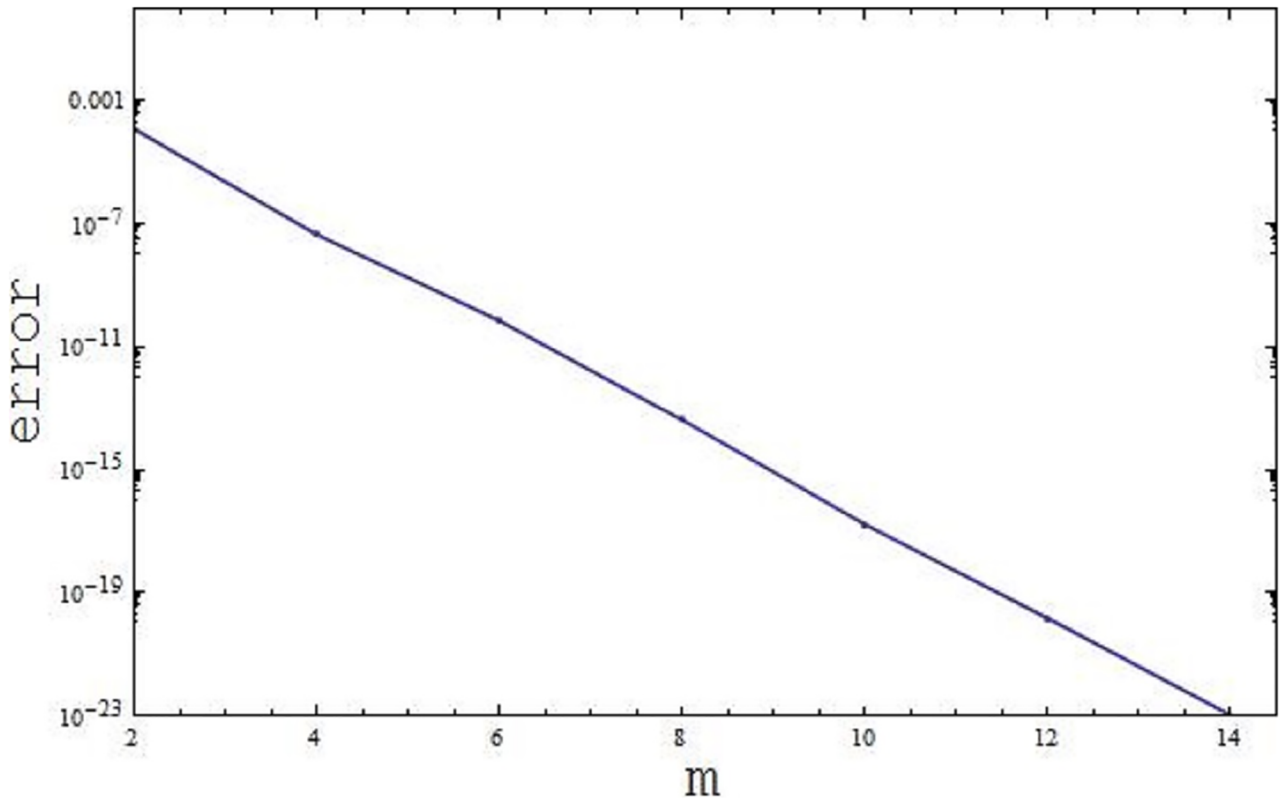

Fig 2. Display the error decay for the 10^{th} order approximation.

https://doi.org/10.1371/journal.pone.0188460.g002

Table 4. Comparison of Nusselt number for the case when $\beta = \lambda = \varepsilon = \gamma = 0$.

Pr	Rashidi [38]	$\frac{\text{OHAM results}}{\text{Re}_x^{-1/2}X^{-1}Nu_x}$	$\frac{\text{BVPh2--Midpoint}}{\text{Re}_x^{-1/2}X^{-1}Nu_x}$
0.72	0.808631	0.808641	0.808639
1.0	1.000000	1.000000	1.000000
3.0	1.923682	1.923690	1.923672
4.0	– – –	2.003170	2.003162
5.0	– – –	2.329810	2.329871
8.0	– – –	– – –	2.541990

https://doi.org/10.1371/journal.pone.0188460.t004

parameter), ε (Curie temperature) and Pr (Prandtl number) are defined as

$$\varepsilon = \frac{T_\infty}{T_c - T_w}, \lambda_1 = h_c\sqrt{\frac{\upsilon_f}{S^2}},\ \ \lambda = \frac{S\mu_f^2}{\rho K_2(T_c - T_w)},\ \ P_m = \frac{\upsilon_f \epsilon}{K_1 S},$$
$$\Pr = \frac{\upsilon_f}{\alpha_f},\ \ \beta = \frac{\gamma_1}{2\pi}\frac{\mu_0 K_2(T_c - T_w)\rho_f}{\mu_f^2},\ \ \gamma = \sqrt{\frac{S\rho_f b^2}{\mu_f}}. \tag{21}$$

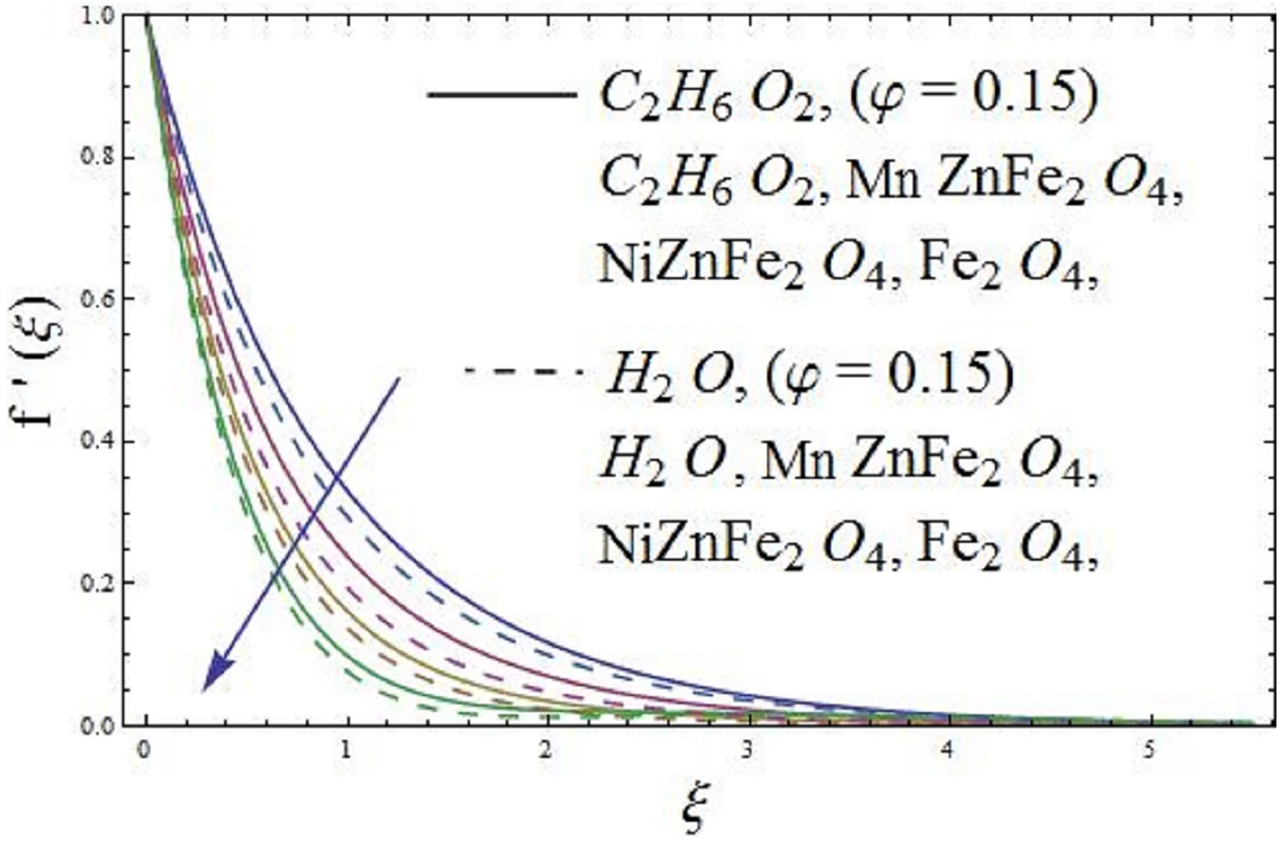

Fig 3. The effect of parameter φ (solid volume fraction) on axial velocity.

https://doi.org/10.1371/journal.pone.0188460.g003

Skin friction coefficient and local Nusselt number are expressed as

$$\begin{aligned} C_f &= \frac{-2\tau_w}{\rho_{nf}U_w^2},\ \tau_w = \mu_{nf}\left.\frac{\partial u}{\partial y}\right|_{y=0}, \\ Nu &= \frac{xk_{nf}}{k_f(T_c - T_w)}\left.\frac{\partial T}{\partial y}\right|_{y=0}. \end{aligned} \tag{22}$$

The dimensionless equations for the skin friction coefficient and Nusselt number (the ratio of convective to conductive heat transfer coefficients) i.e. local surface heat flux

$$\begin{aligned} \frac{1}{2}\mathrm{Re}_x^{1/2}C_f &= \frac{1}{(1-\varphi)^{2.5}}f''(0), \\ \mathrm{Re}_x^{-1/2}Nu_x &= -\frac{\lambda_1 k_{nf}}{k_f}\left(1 + \frac{1}{\theta_1(0) + \zeta^2\theta_2(0)}\right). \end{aligned} \tag{23}$$

$\mathrm{Re}_x^{1/2}C_f$ is the local skin friction coefficient and $\mathrm{Re}_x^{-1/2}Nu_x$ is the Nusselt number, in which $\mathrm{Re}_x = xU_w(x)/\upsilon_f = Sx^2/\upsilon_f$ is a local Reynolds number (i.e. the ratio of inertial to viscous forces) depends on the stretching velocity $U_w(x)$.

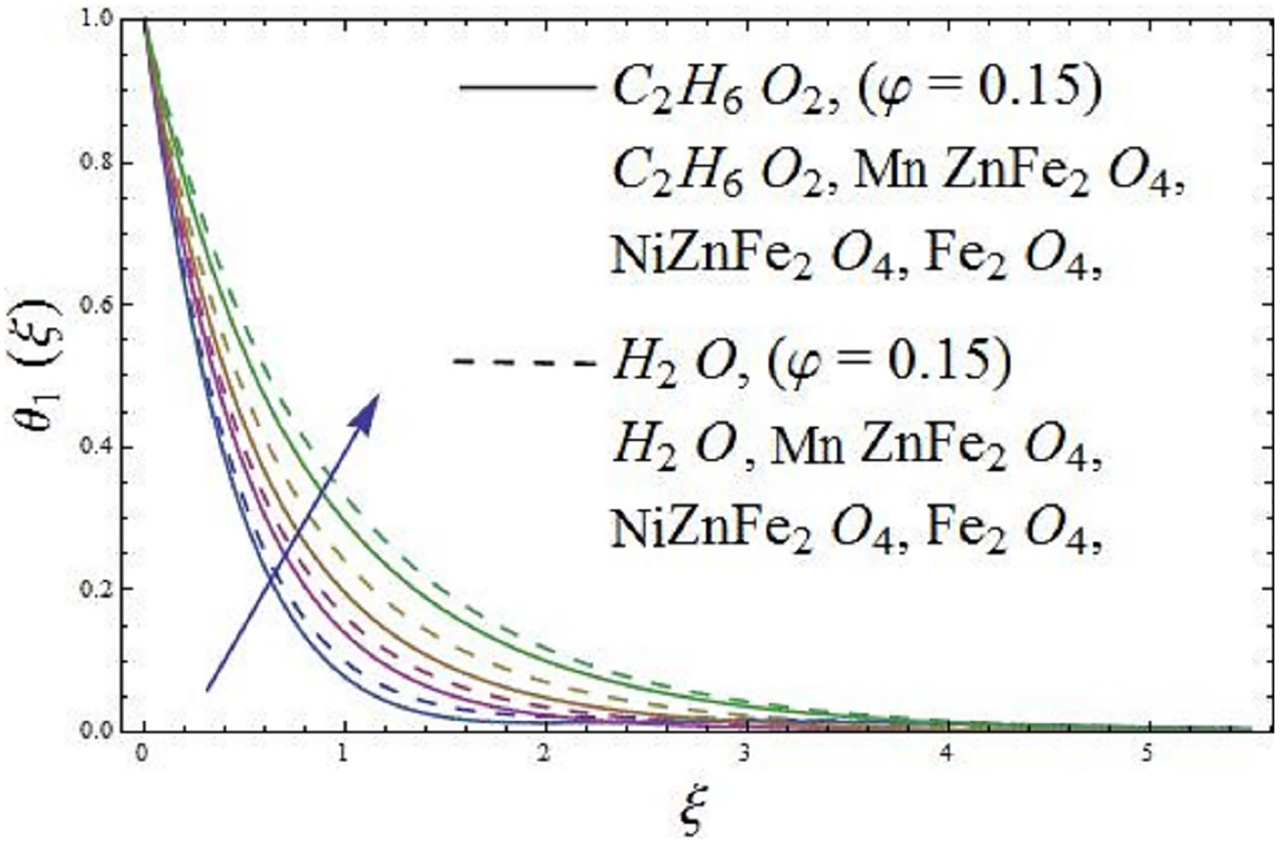

Fig 4. The effect of parameter φ (solid volume fraction) on temperature field.

https://doi.org/10.1371/journal.pone.0188460.g004

BVPh2—Midpoint method (Maple) and optimal homotopy analysis method (Mathematica 9.0) are implemented in the present analysis for the solution of the non-linear ordinary momentum Eq 16 and thermal energy Eqs 17 and 18 subjected to the admissible boundary conditions in Eqs 19 and 20. These techniques are utilized to get the solutions for highly non—linear equations. The optimal HAM [36, 37] gives better results as compared to perturbation techniques and other conventional investigative techniques. The generality of the optimal HAM often allows for good convergence of the solution over larger spatial and parameter domains. Firstly, the optimal HAM gives us a remarkable flexibility to pick the equation type of linear sub-problems. Secondly, the optimal HAM works regardless of the possibility that there don't exist any small/large physical parameters in determining equations and boundary/initial conditions. Particularly, unlike perturbation and other analytic techniques, the optimal HAM gives us an advantageous approach to guarantee the convergence of series solution by method of presenting the supposed convergence control parameter into the series solution. Moreover, the optimal HAM utilize the homotopy/auxiliary parameter only on a theoretical level to depict that a nonlinear system of differential equations may be divided into a set of linear system of differential equations which are solved analytically, while the continuation methods require solving a discrete linear system as the homotopy parameter is varied to solve the nonlinear system. The respective linear operators and their relating initial guesses for the

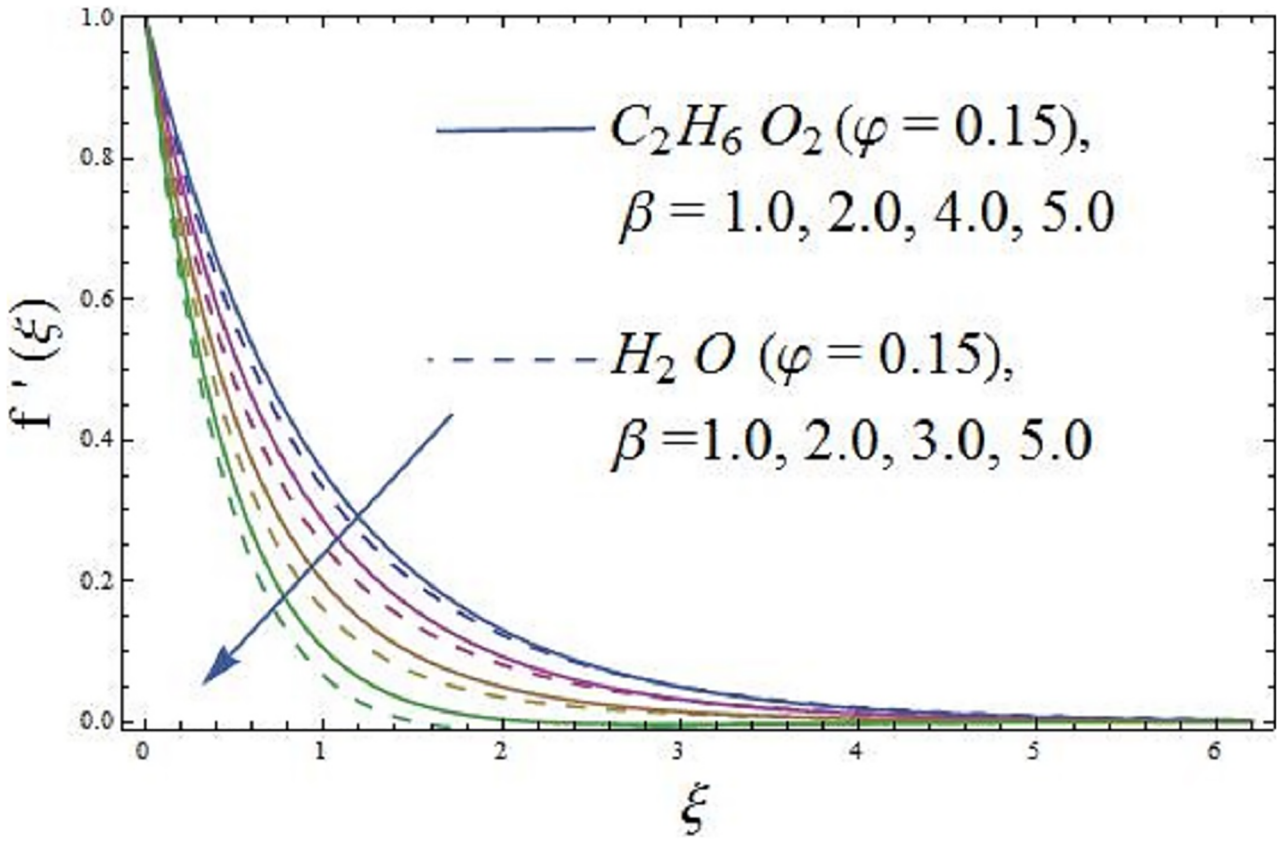

Fig 5. The effect of parameter β (ferrohydrodynamic interaction) on axial velocity.

https://doi.org/10.1371/journal.pone.0188460.g005

boundary value problem are

$$L_f(f) = \frac{d^3 f}{d\xi^3} + \frac{d^2 f}{d\xi^2}, L_{\theta_1}(\theta_1) = \frac{d^2\theta_1}{d\xi^2} - \theta_1, L_{\theta_2}(\theta_2) = \frac{d^2\theta_2}{d\xi^2} - \theta_2, \tag{24}$$

$$f_0(\xi) = 1 - \exp(-\xi), \ \ \theta_{1_0}(\xi) = \frac{\lambda_1}{1-\lambda_1}\exp(-\xi), \tag{25}$$

$$\theta_{2_0}(\xi) = \xi\exp(-\xi), \tag{26}$$

where $L_f(f)$, $L_{\theta_1}(\theta_1)$, and $L_{\theta_2}(\theta_2)$ symbolizes the linear operators, on the other hand $f_0(\xi)$, $\theta_{1_0}(\xi)$, and $\theta_{2_0}(\xi)$ illustrate the respective initial guesses of f, θ_1, and θ_2.

4 Convergence analysis for optimal HAM solution

The auxiliary parameters $\hbar_f$, $\hbar_{\theta_1}$, and $\hbar_{\theta_2}$ have a leading purpose of controlling the convergence of homotopic solutions. To get convergent solutions, we take suggested values of these parameters. For this reason, residual errors are noticed for momentum, and thermal energy

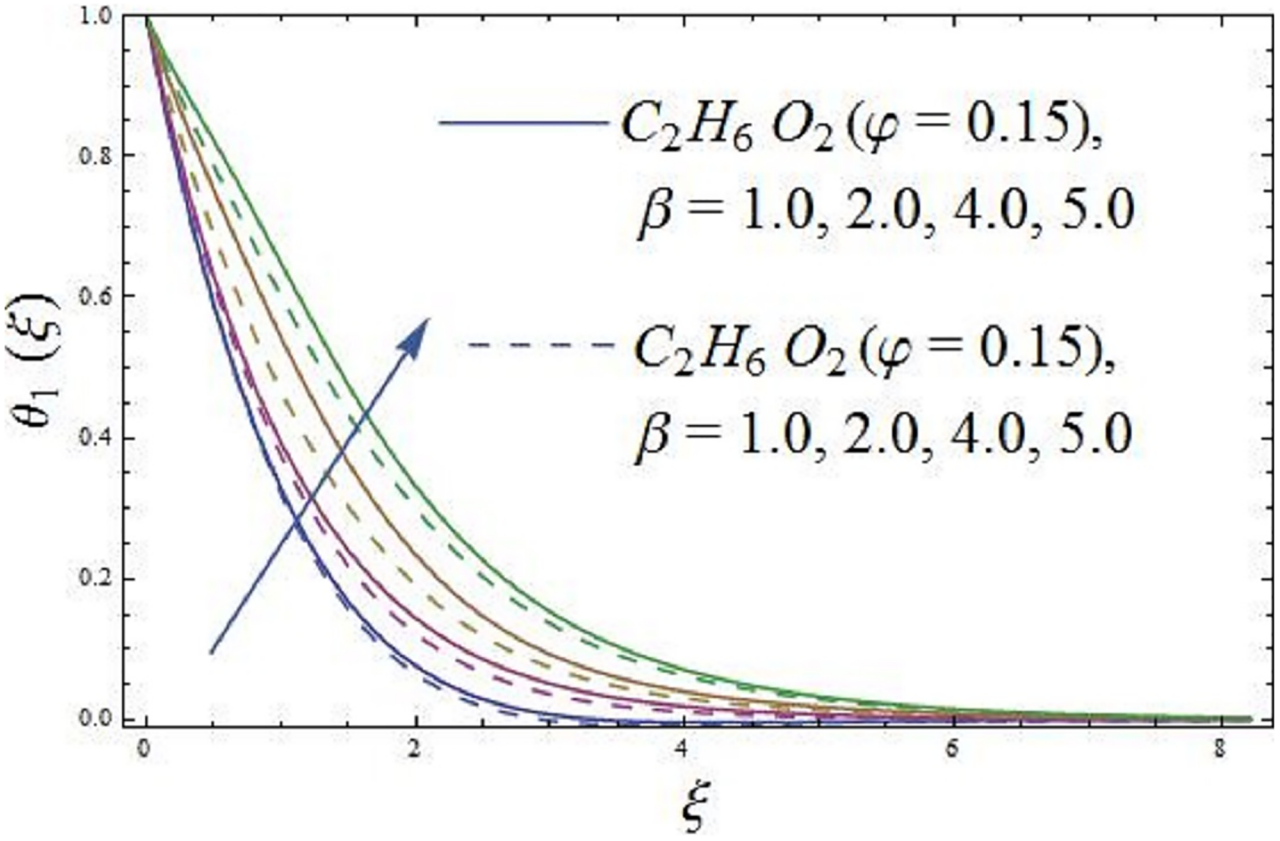

Fig 6. The effect of parameter β (ferrohydrodynamic interaction) on temperature field.

https://doi.org/10.1371/journal.pone.0188460.g006

equations by initiating the expressions given below,

$$\Delta_m^f = \int_0^1 [\mathcal{R}_m^f(\xi, \hbar_f)]^2 d\xi, \tag{27}$$

$$\Delta_m^{\theta_1} = \int_0^1 [\mathcal{R}_m^{\theta_1}(\xi, \hbar_{\theta_1})]^2 d\xi, \tag{28}$$

$$\Delta_m^{\theta_2} = \int_0^1 [\mathcal{R}_m^{\theta_2}(\xi, \hbar_{\theta_2})]^2 d\xi, \tag{29}$$

The convergence of the parametric values is displayed by OHAM, listed in the following Tables 2 and 3, using the values of the parameters $\beta = 1.2$, $\lambda = 0.01$, $\lambda_1 = 0.5$, Pr = 204, $\varphi = 0.1$, and $\gamma = 0.1$.

The graphical representation for the 10^{th} order approximation display the error decay in the following Fig 2.

Here Δ_m^t indicate the total discrete squared residual error.

$$\Delta_m^t = \Delta_m^f + \Delta_m^{\theta_1} + \Delta_m^{\theta_2}. \tag{30}$$

Here the Δ_m^t is used to obtain the optimal convergence control parameters.

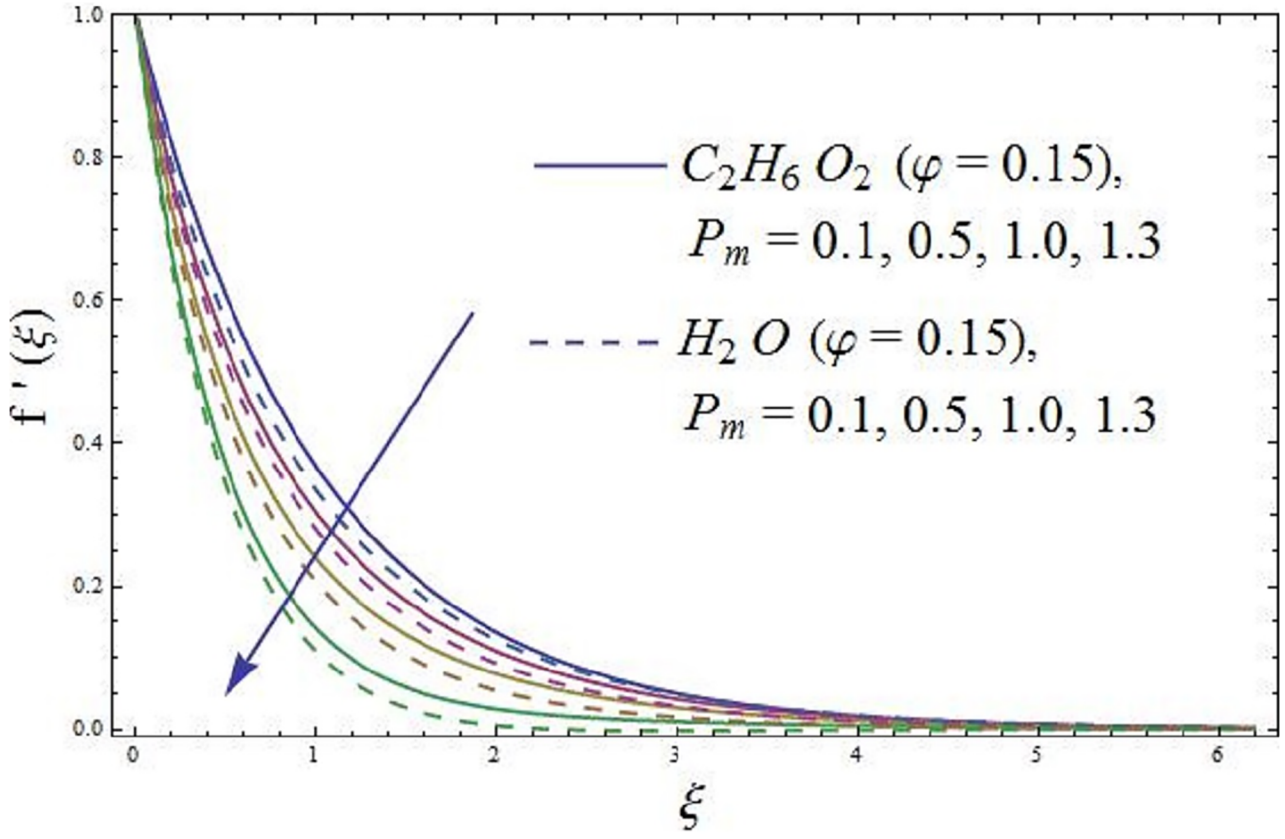

Fig 7. Impact of P_m (Porosity parameter) on axial velocity.

https://doi.org/10.1371/journal.pone.0188460.g007

5 Results and discussion

This section contains the physical interpretation of sundry parameters on the flow field. The effects of dimensionless emerging parameters β (ferrohydrodynamic interaction), P_m (porosity parameter), φ (solid volume fraction of nanofluid), λ_1 (the conjugate parameter of Newtonian heating), and Pr (Prandtl number) are analyzed. Moreover, rest of the materialize parameters in the flow problem are considered fixed. The fixed values of these parameters are taken as $\lambda = 0.01$, $\varepsilon = 2.0$, $\gamma_1 = 1.0$. The boundary value problem is solved numerically and analytically via BVPh2-Midpoint method and optimal homotopy analysis method (OHAM) respectively. The accuracy of the present optimal HAM and BVPh2—midpoint method is tested by comparing $\theta_1'(0)$ values with those of Rashidi [38] for pure fluid that is tabulated in Table 4. An excellent agreement between the result is found for special case of the present problem. The boundary layer flow of a ferromagnetic $NiZnFe_2O_4$—$C_2H_6O_2$, $NiZnFe_2O_4$—H_2O, $MnZnFe_2O_4$—$C_2H_6O_2$, $MnZnFe_2O_4$—H_2O, Fe_2O_4—$C_2H_6O_2$, and Fe_2O_4—H_2O nanofluids with nanoparticles are investigated. In order to get an obvious insight of the existing flow problem, the results are dig out for the axial velocity, temperature field, skin friction coefficient, and Nusselt number graphically. The analysis is carried out in the presence of magnetic dipole.

The influence of parameter φ (solid volume fraction of nanofluid) of the ferromagnetic $NiZnFe_2O_4$—$C_2H_6O_2$, $NiZnFe_2O_4$—H_2O, $MnZnFe_2O_4$—$C_2H_6O_2$, $MnZnFe_2O_4$—H_2O, Fe_2O_4—$C_2H_6O_2$, and Fe_2O_4—H_2O nanofluids are depicted in Figs 3 and 4 on the dimensionless axial velocity and temperature field. It is evident from Fig 3 that the axial velocity of the

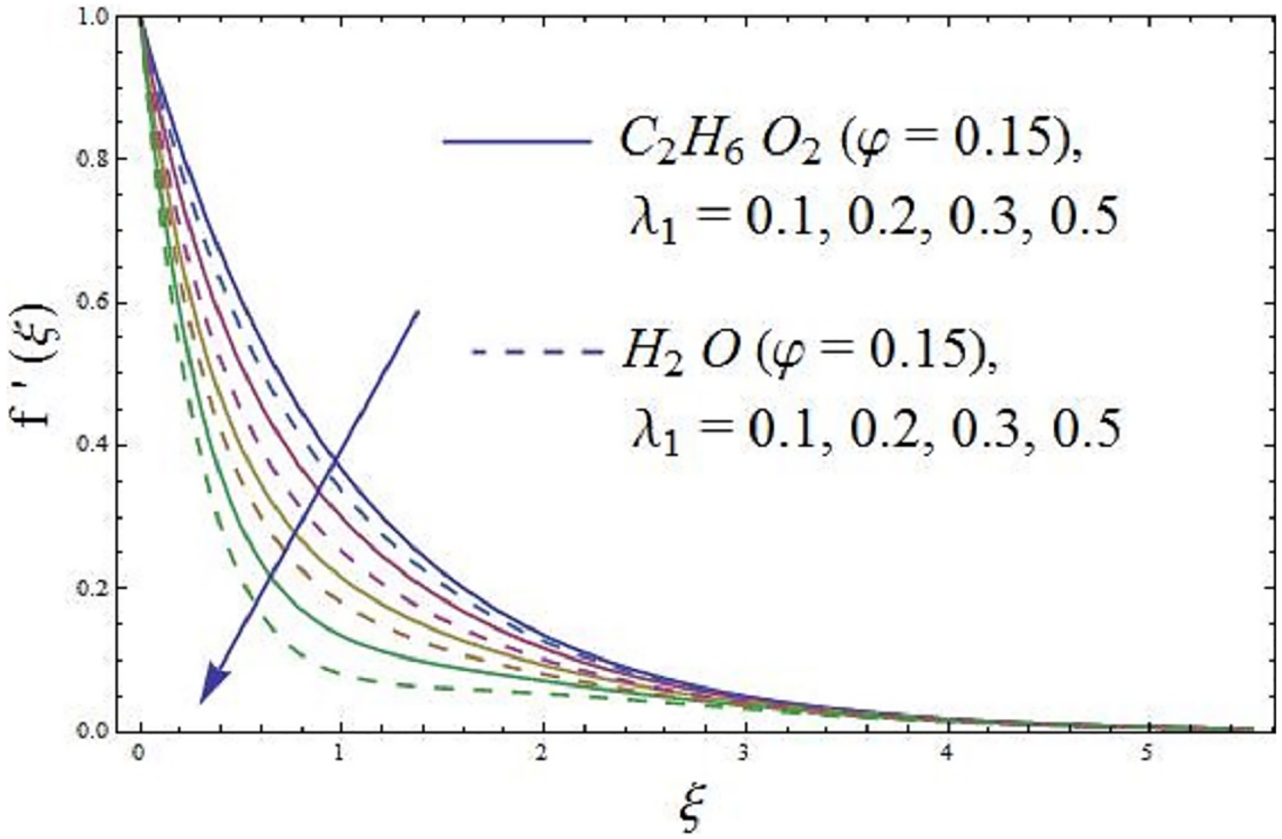

Fig 8. Effect of parameter λ_1 (the conjugate parameter of Newtonian heating) on axial velocity.

https://doi.org/10.1371/journal.pone.0188460.g008

respective nanofluids decreases with an increase in parameter φ (solid volume fraction of nanofluid). The axial velocity reduces as we move far away from the surface. In fact, an increase in parameter φ (solid volume fraction of nanofluid) causes to concentrates the ferromagnetic fluid which consequently produces resistance to the fluid motion and as a result, the axial velocity reduces for both the base fluids, i.e., (water and ethylene glycol). The presence of magnetic dipole provides attraction to the ferrites nanoparticles due to which the axial velocity of the ferromagnetic nanofluids slows down. It means that magnetic dipole plays a vital role in reducing the movements of fluid particles. Further, Fig 3 depicts that Fe_2O_4 (magnetite ferrite) nanoparticles are more magnetized as compared to $NiZnFe_2O_4$ (Nickel zinc ferrite) and $MnZnFe_2O_4$ (Manganese zinc ferrite) nanoparticles. The more magnetization, the more will be resistance produced by the magnetic dipole to the fluid particles, as a result, it is depicted that Fe_2O_4—$C_2H_6O_2$ and Fe_2O_4—H_2O ferromagnetic nanofluids have low velocity as compared to the ferromagnetic $NiZnFe_2O_4$—$C_2H_6O_2$, $NiZnFe_2O_4$—H_2O, $MnZnFe_2O_4$—$C_2H_6O_2$, and $MnZnFe_2O_4$—H_2O nanofluids. The characteristics of parameter φ (solid volume fraction of nanofluid) on temperature field of the ferromagnetic $NiZnFe_2O_4$—$C_2H_6O_2$, $NiZnFe_2O_4$—H_2O, $MnZnFe_2O_4$—$C_2H_6O_2$, $MnZnFe_2O_4$—H_2O, Fe_2O_4—$C_2H_6O_2$, and Fe_2O_4—H_2O nanofluids in presence of magnetic dipole are delineated in Fig 4. It is illustrated that temperature field of Fe_2O_4—$C_2H_6O_2$ and Fe_2O_4—H_2O is higher than $NiZnFe_2O_4$—$C_2H_6O_2$, $NiZnFe_2O_4$—H_2O, $MnZnFe_2O_4$—$C_2H_6O_2$, and $MnZnFe_2O_4$—H_2O nanofluids in presence of magnetic dipole. It is due to the fact that the thermal conductivity of Fe_2O_4 (magnetite ferrite) nanoparticles is higher than the thermal conductivity of $NiZnFe_2O_4$ (Nickel zinc ferrite) and

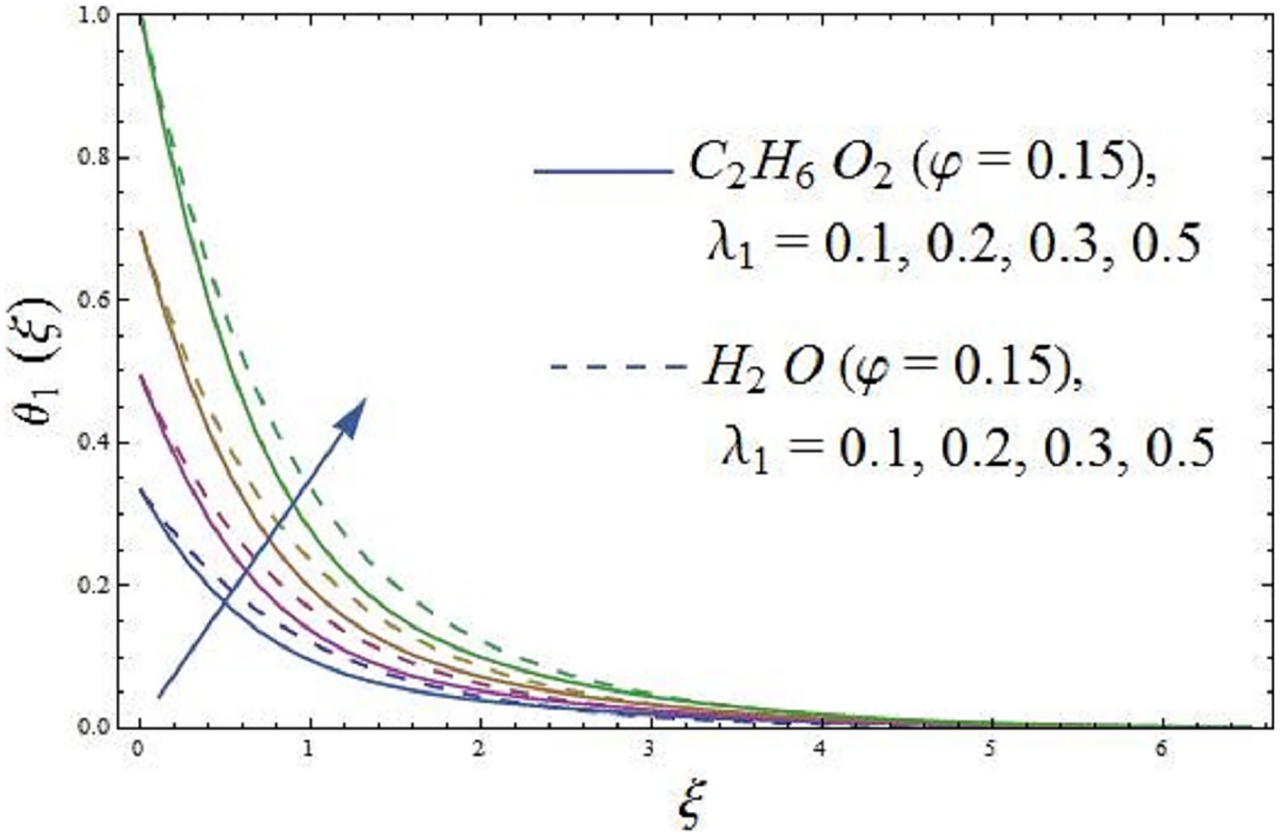

Fig 9. Effect of parameter λ_1 (the conjugate parameter of Newtonian heating) on temperature field.

https://doi.org/10.1371/journal.pone.0188460.g009

$MnZnFe_2O_4$ (manganese zinc ferrite) nanoparticles. Moreover, the presence of magnetic dipole makes higher the temperature field until the temperature of the fluid reach to the Curie temperature T_c of the fluid. It is due to the fact that magnetic dipole produces more resistance to the Fe_2O_4 (magnetite ferrite) nanoparticles as compared to $NiZnFe_2O_4$ (Nickel zinc ferrite) and $MnZnFe_2O_4$ (manganese zinc ferrite) nanoparticles, which results in the enhancement of temperature field. If the temperature of the ferrite nanoparticles is higher than the Curie temperature T_c then these ferrite nanoparticles lose their magnetization and there will be no attraction for ferrite nanoparticles whose temperature is higher than the Curie temperature T_c.

The impact of parameter β (ferrohydrodynamic interaction) is displayed in Figs 5 and 6. The existence of parameters γ_1 (dimensionless distance from origin to center of magnetic dipole), ε (Curie temperature), and β (ferrohydrodynamic interaction) is necessary to hold the impact of ferromagnetic effect on the boundary layer flow. The presence of Fe_2O_4 (magnetite ferrite), $NiZnFe_2O_4$ (Nickel zinc ferrite) and $MnZnFe_2O_4$ (manganese zinc ferrite) nanoparticles in a viscous carrier fluid corresponds to ferromagnetic nanofluid, because of which viscosity of the fluid enhances and as a result, the axial velocity reduces for enlarging values of parameter β (ferrohydrodynamic interaction) as shown in Fig 5. The influence of β (ferrohydrodynamic interaction) on axial velocity is carried out for the ferromagnetic $NiZnFe_2O_4$—$C_2H_6O_2$, $NiZnFe_2O_4$—H_2O, $MnZnFe_2O_4$—$C_2H_6O_2$, $MnZnFe_2O_4$—H_2O, Fe_2O_4—$C_2H_6O_2$, and Fe_2O_4—H_2O nanofluids. It is noticed that the presence of magnetic dipole makes a rapid reduction in the axial velocity of the ferromagnetic nanofluids when water is used as base fluid.

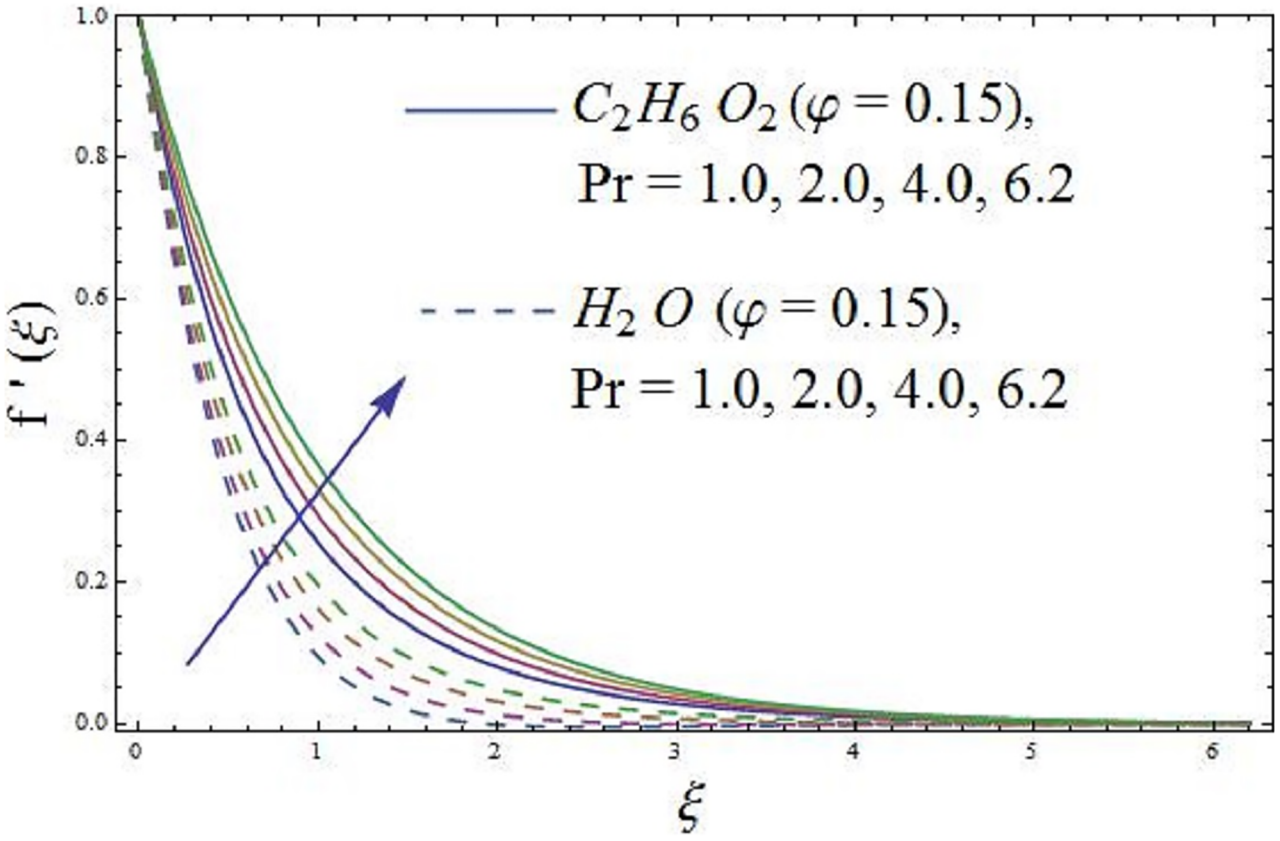

Fig 10. Impact of parameter Pr (Prandtl number) on axial velocity.

https://doi.org/10.1371/journal.pone.0188460.g010

The physical interpretation is that the magnetic dipole attracts the ferrite Fe_2O_4 (magnetite ferrite), $NiZnFe_2O_4$ (Nickel zinc ferrite) and $MnZnFe_2O_4$ (manganese zinc ferrite) nanoparticles which result in the enhancement of the viscosity of the nanofluid inside the boundary layer and as a result, the axial velocity slows down. The highest velocity is observed for the $C_2H_6O_2$ (ethylene glycol, when $\varphi = 0$) and H_2O (water, when $\varphi = 0$), whereas the lowest axial velocity is observed for the Fe_2O_4—$C_2H_6O_2$ (magnetite ferrite-ethylene glycol, when $\varphi = 0.15$) and Fe_2O_4—H_2O (magnetite ferrite-water, when $\varphi = 0.15$) nanofluids as evident in Fig 5. Fig 6 characterizes the influence of parameter β (ferrohydrodynamic interaction) on temperature field. It is depicted that the larger values of parameter β (ferrohydrodynamic interaction) leads to enhance the temperature of the nanofluid in presence of the magnetic dipole. It is because of the interaction between an action of a magnetic field and movements of Fe_2O_4 (magnetite ferrite), $NiZnFe_2O_4$ (Nickel zinc ferrite) and $MnZnFe_2O_4$ (manganese zinc ferrite) nanoparticles. The interaction between magnetic field action and Fe_2O_4 (magnetite ferrite), $NiZnFe_2O_4$ (Nickel zinc ferrite) and $MnZnFe_2O_4$ (manganese zinc ferrite) nanoparticles thinning the axial velocity thereby enhancing frictional heating among fluid layers, that leads to rise thermal boundary layer i.e., the reduction in movements of Fe_2O_4 (magnetite ferrite), $NiZnFe_2O_4$ (Nickel zinc ferrite) and $MnZnFe_2O_4$ (manganese zinc ferrite) nanoparticles results in the enhancement of temperature field.

The effect of parameter P_m (Porosity) in the flow of ferromagnetic $NiZnFe_2O_4$—$C_2H_6O_2$, $NiZnFe_2O_4$—H_2O, $MnZnFe_2O_4$—$C_2H_6O_2$, $MnZnFe_2O_4$—H_2O, Fe_2O_4—$C_2H_6O_2$, and

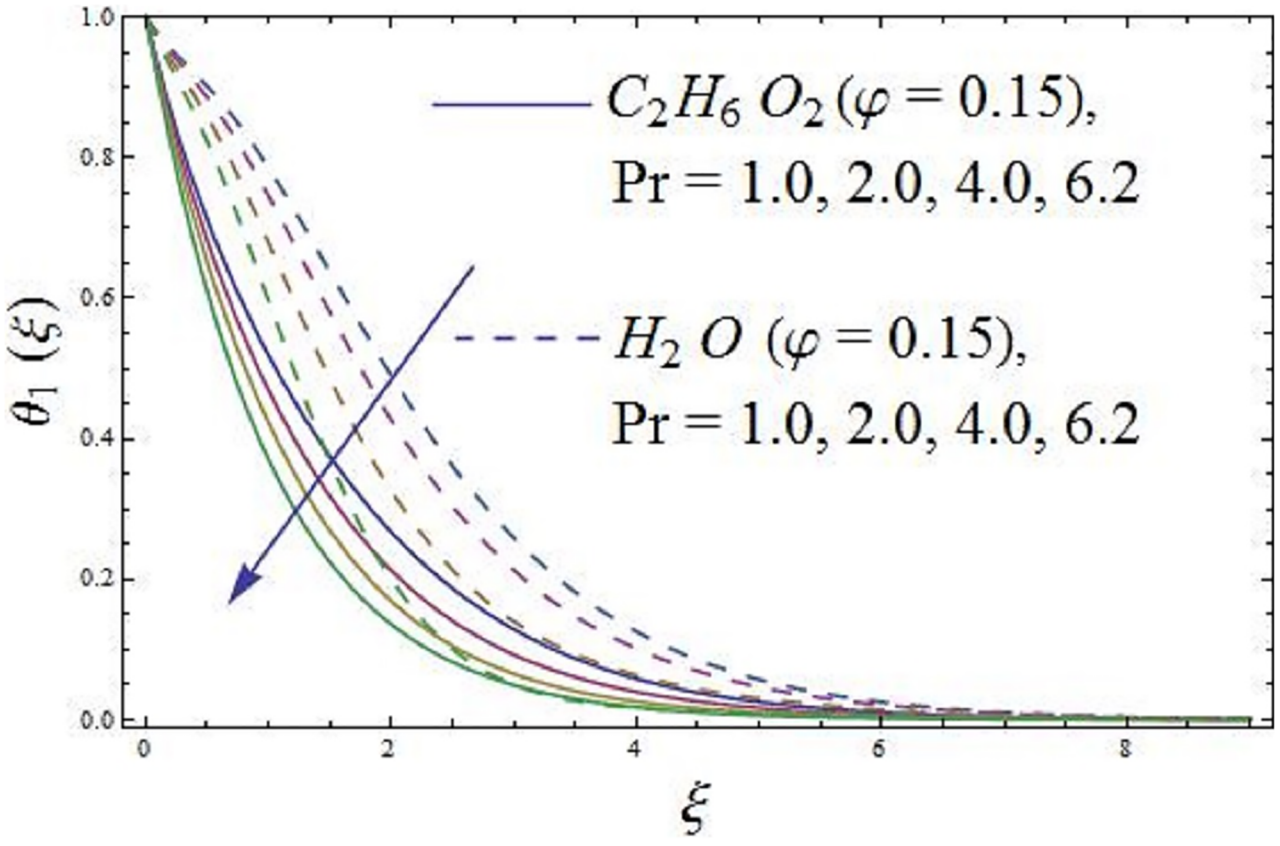

Fig 11. Impact of parameter Pr (Prandtl number) on temperature field.

https://doi.org/10.1371/journal.pone.0188460.g011

Fe_2O_4—H_2O nanofluids is observed in Fig 7. The existence of parameters P_m (Porosity) in the presence of Fe_2O_4 (magnetite ferrite), $NiZnFe_2O_4$ (Nickel zinc ferrite) and $MnZnFe_2O_4$ (manganese zinc ferrite) nanoparticles in a viscous carrier ferromagnetic nanofluid slow down the axial velocity and as a result the axial velocity reduces for enlarging values of parameter P_m (Porosity) as shown in Fig 7. It is depicted that for ferrites-water based ferromagnetic nanofluid in the presence of magnetic dipole, the axial velocity reduces rapidly. The physical interpretation is that an increase in P_m (Porosity) causes to produce more resistance to the fluid particles, and the magnetic dipole attracts the ferrite Fe_2O_4 (magnetite ferrite), $MnZnFe_2O_4$ (manganese zinc ferrite), and $NiZnFe_2O_4$ (Nickel zinc ferrite) nanoparticles which result in the enhancement of the viscosity of the nanofluid inside the nano boundary layer and as a result the axial velocity slow down. The highest velocity is observed for the $C_2H_6O_2$ (ethylene glycol, when $\varphi = 0$) and H_2O (water, when $\varphi = 0$), whereas the lowest axial velocity is observed for the Fe_2O_4—$C_2H_6O_2$ (magnetite ferrite-ethylene glycol, when $\varphi = 0.15$) and Fe_2O_4—H_2O (magnetite ferrite-water, when $\varphi = 0.15$) nanofluids as evident in Fig 7.

The influence of conjugate parameter λ_1 of Newtonian heating on axial velocity and temperature profile are addressed in Figs 8 and 9. It is disclosed from Fig 8 that an increase in the λ_1 (conjugate parameter) prompts change in the axial velocity of the ferromagnetic $NiZnFe_2O_4$—$C_2H_6O_2$, $NiZnFe_2O_4$—H_2O, $MnZnFe_2O_4$—$C_2H_6O_2$, $MnZnFe_2O_4$—H_2O, Fe_2O_4—$C_2H_6O_2$, and Fe_2O_4—H_2O nanofluids, the consequence indicate that the axial velocity and relative nano boundary layer are decreasing functions of λ_1 (conjugate parameter) i.e., the axial velocity is reduces. It is inspected that the response velocity reduces with rise (increasing

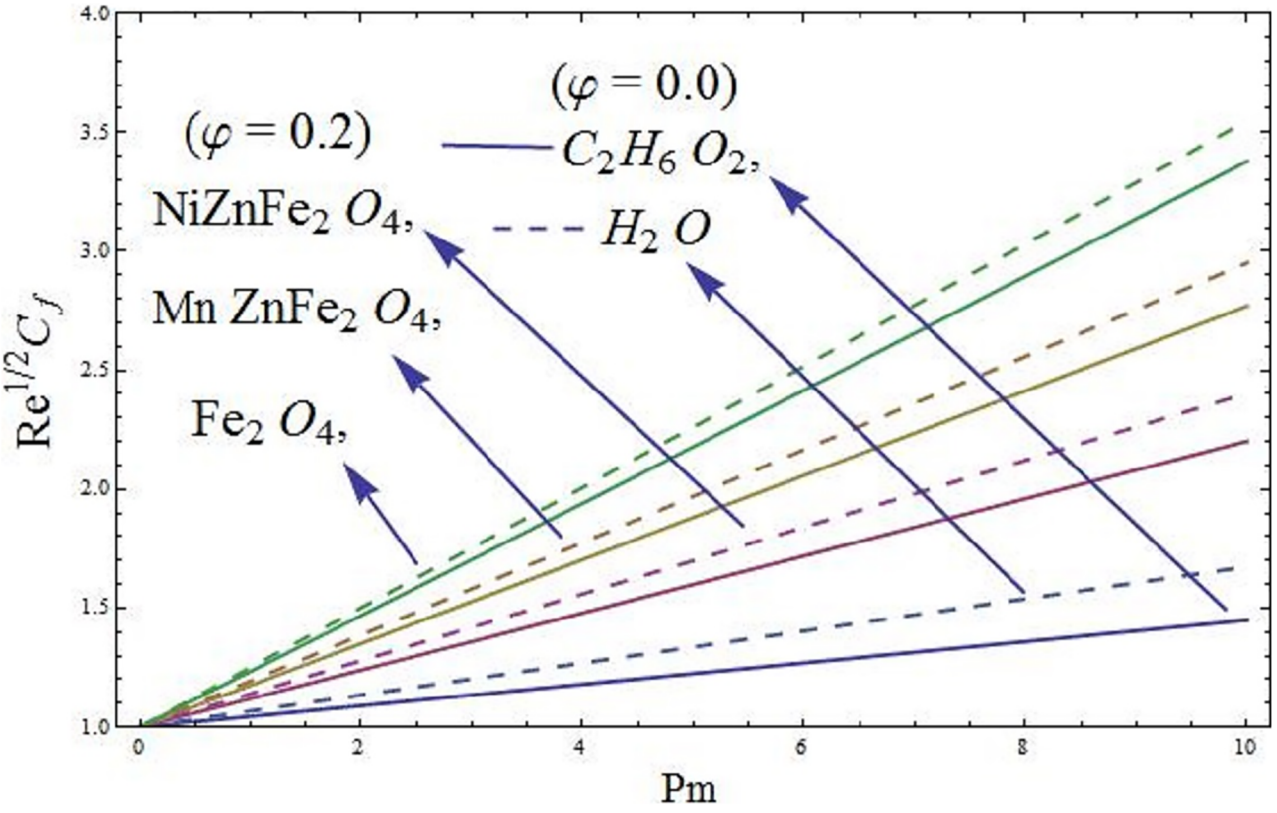

Fig 12. Wall shear stress versus P_m.

https://doi.org/10.1371/journal.pone.0188460.g012

values of λ_1) of an elastic force of the working fluid. The impacts of λ_1 (conjugate parameter) on temperature field is characterized in Fig 9. It is revealed that an increase in λ_1 (conjugate parameter) increases the heat transfer coefficient which improves the temperature of the ferromagnetic $NiZnFe_2O_4$—$C_2H_6O_2$, $NiZnFe_2O_4$—H_2O, $MnZnFe_2O_4$—$C_2H_6O_2$, $MnZnFe_2O_4$—H_2O, Fe_2O_4—$C_2H_6O_2$, and Fe_2O_4—H_2O nanofluids. Further, thermal boundary layer thickness increases. It is likewise noticed that temperature at the surface is higher for large values of λ_1 (conjugate parameter).

The parameter Pr (Prandtl number) in the thermal energy equation effect their respective thermal boundary layer thickness. It is depicted in Fig 10 that higher values of parameter Pr (Prandtl number) enhances the axial velocity. Fig 11 exhibit the influence of parameter Pr (Prandtl number) temperature field of the ferromagnetic $NiZnFe_2O_4$—$C_2H_6O_2$, $NiZnFe_2O_4$—H_2O, $MnZnFe_2O_4$—$C_2H_6O_2$, $MnZnFe_2O_4$—H_2O, Fe_2O_4—$C_2H_6O_2$, and Fe_2O_4—H_2O nanofluids. It is investigated that the temperature field along thermal boundary layer thickness reduces for higher values of parameter Pr (Prandtl number) in presence of the magnetic dipole. A higher penetrating depth of temperature field is noticed at Pr = 1.0, as compared with Pr = 6.2, which results in the reduction of thermal diffusivity as parameter Pr (Prandtl number) rises. Reduction in thermal diffusivity leads to diffused heat away from the heated sheet and by the way, the temperature gradient at the surface is enhanced. This phenomenon decreases the ability of energy that decline the thickness of thermal boundary layer and enhance the axial velocity. The values assigned to remaining parameters are $\lambda = 0.01$, $\lambda_1 = 0.3$, $\beta = 1.2$, Pr = 6.96, $P_m = 0.5$, and $\gamma = 0.1$.

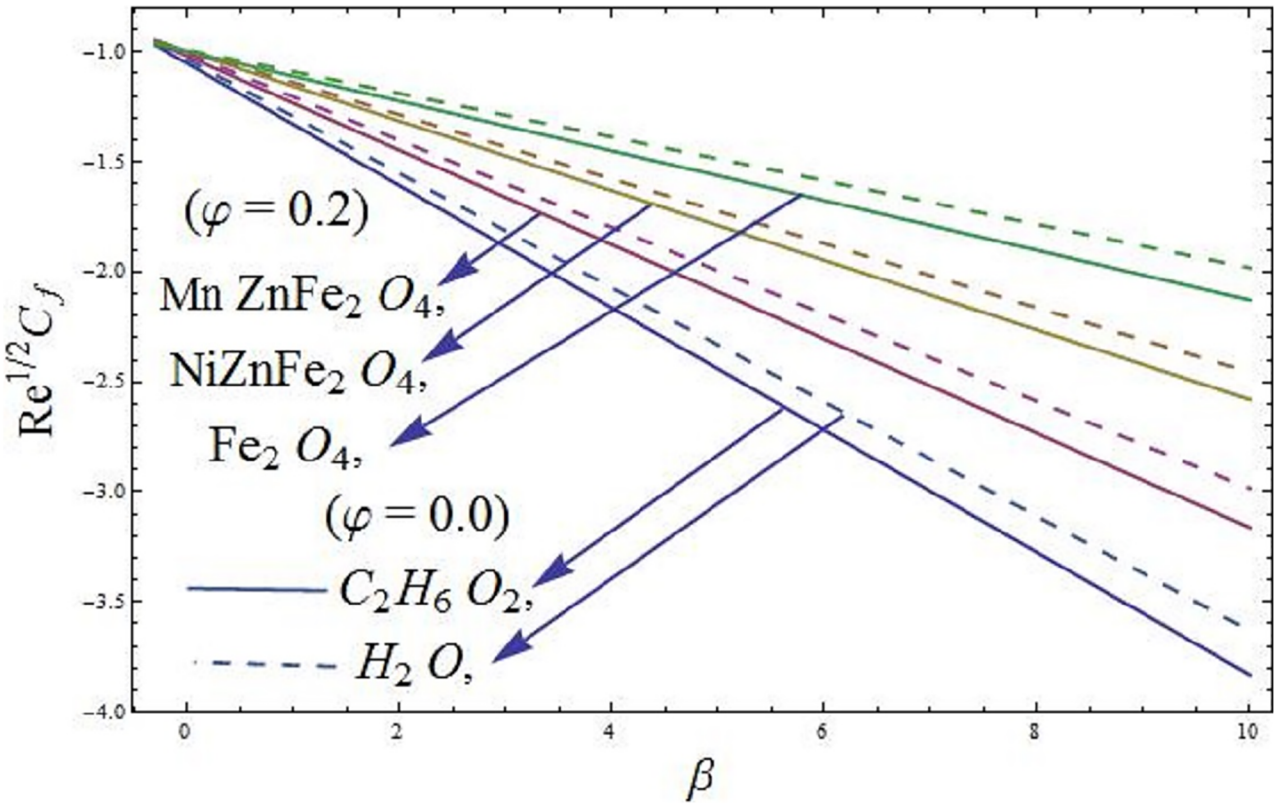

Fig 13. Wall shear stress versus β.

https://doi.org/10.1371/journal.pone.0188460.g013

5.1 Skin friction coefficient and local Nusselt number

The mathematical relations for skin friction coefficient and Nusselt number are given in Eqs 22 and 23. The influence of parameter φ (solid volume fraction of nanofluid) on wall shear stress of the ferromagnetic $NiZnFe_2O_4$—$C_2H_6O_2$, $NiZnFe_2O_4$—H_2O, $MnZnFe_2O_4$—$C_2H_6O_2$, $MnZnFe_2O_4$—H_2O, Fe_2O_4—$C_2H_6O_2$, and Fe_2O_4—H_2O nanofluids in presence of the magnetic dipole are evident in Fig 12. It is seen that the presence of water based ferrite nanoparticles reduces the wall shear stress as compared to the case when ethylene glycol-based ferrite nanoparticles are used. The skin friction coefficient is analyzed in the presence of magnetic dipole. Since we know that the magnetic dipole attracts the Fe_2O_4 (magnetite ferrite), $NiZnFe_2O_4$ (Nickel zinc ferrite) and $MnZnFe_2O_4$ (manganese zinc ferrite) nanoparticles which result in the enhancement of the viscosity of the nanofluid inside the boundary layer and yet the wall shear stress increases. The lowest wall shear stress is depicted for the $C_2H_6O_2$ (ethylene glycol, when $\varphi = 0$) and H_2O (water, when $\varphi = 0$) and the highest wall shear stress is observed for the Fe_2O_4—$C_2H_6O_2$ (magnetite ferrite-ethylene glycol, when $\varphi = 0.15$) and Fe_2O_4—H_2O (magnetite ferrite-water, when $\varphi = 0.15$) nanofluids as evident in Figs 12 and 13. Moreover, φ (solid volume fraction of nanofluid) on wall shear stress of the ferromagnetic $NiZnFe_2O_4$—$C_2H_6O_2$, $NiZnFe_2O_4$—H_2O, $MnZnFe_2O_4$—$C_2H_6O_2$, $MnZnFe_2O_4$—H_2O, Fe_2O_4—$C_2H_6O_2$, and Fe_2O_4—H_2O nanofluids in the presence of the magnetic dipole via heat transfer rate are analyzed in Figs 14 and 15. It is scrutinized from Fig 14 that the heat transfer rate reduces for ferromagnetic $NiZnFe_2O_4$—$C_2H_6O_2$, $NiZnFe_2O_4$—H_2O, $MnZnFe_2O_4$—$C_2H_6O_2$, $MnZnFe_2O_4$—H_2O, Fe_2O_4—$C_2H_6O_2$, and Fe_2O_4—H_2O nanofluids. The fast reduction in heat

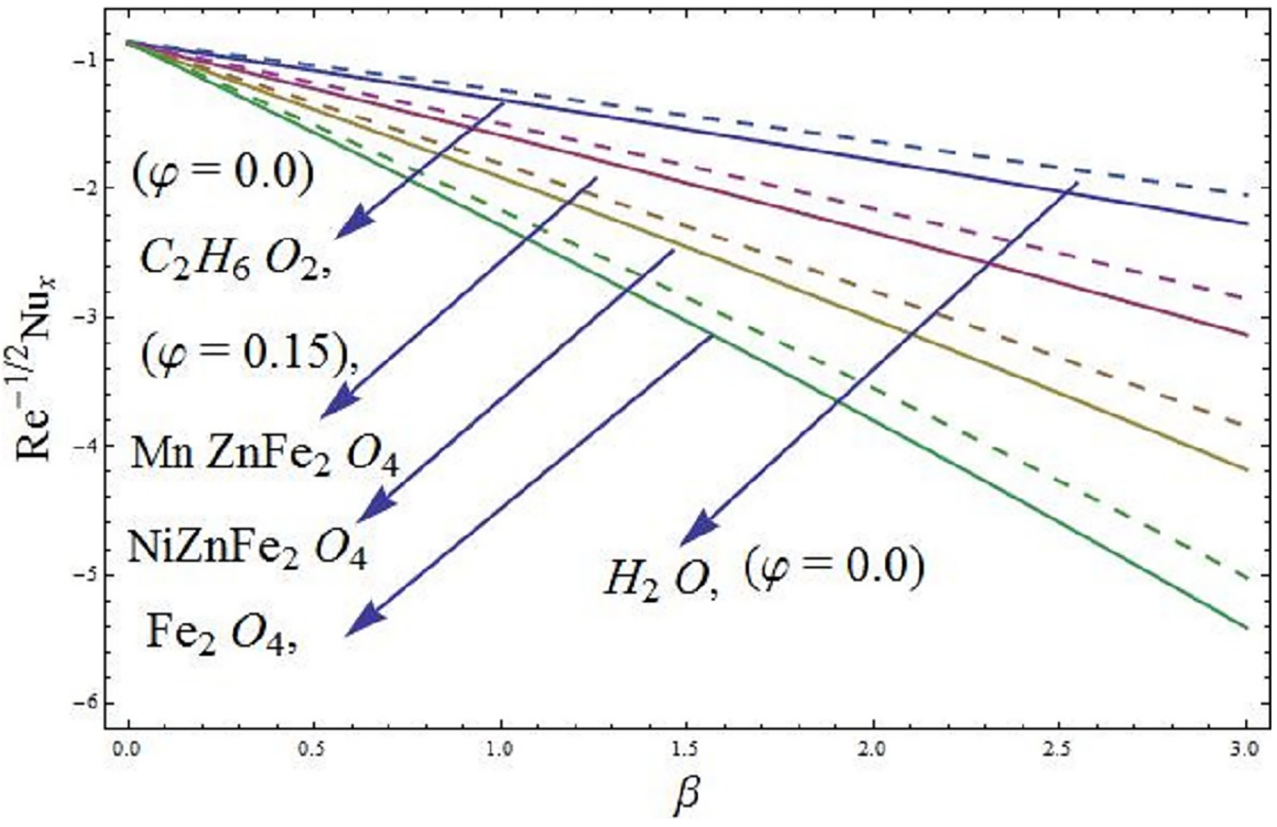

Fig 14. Heat transfer rate versus β (ferrohydrodynamic interaction parameter).

https://doi.org/10.1371/journal.pone.0188460.g014

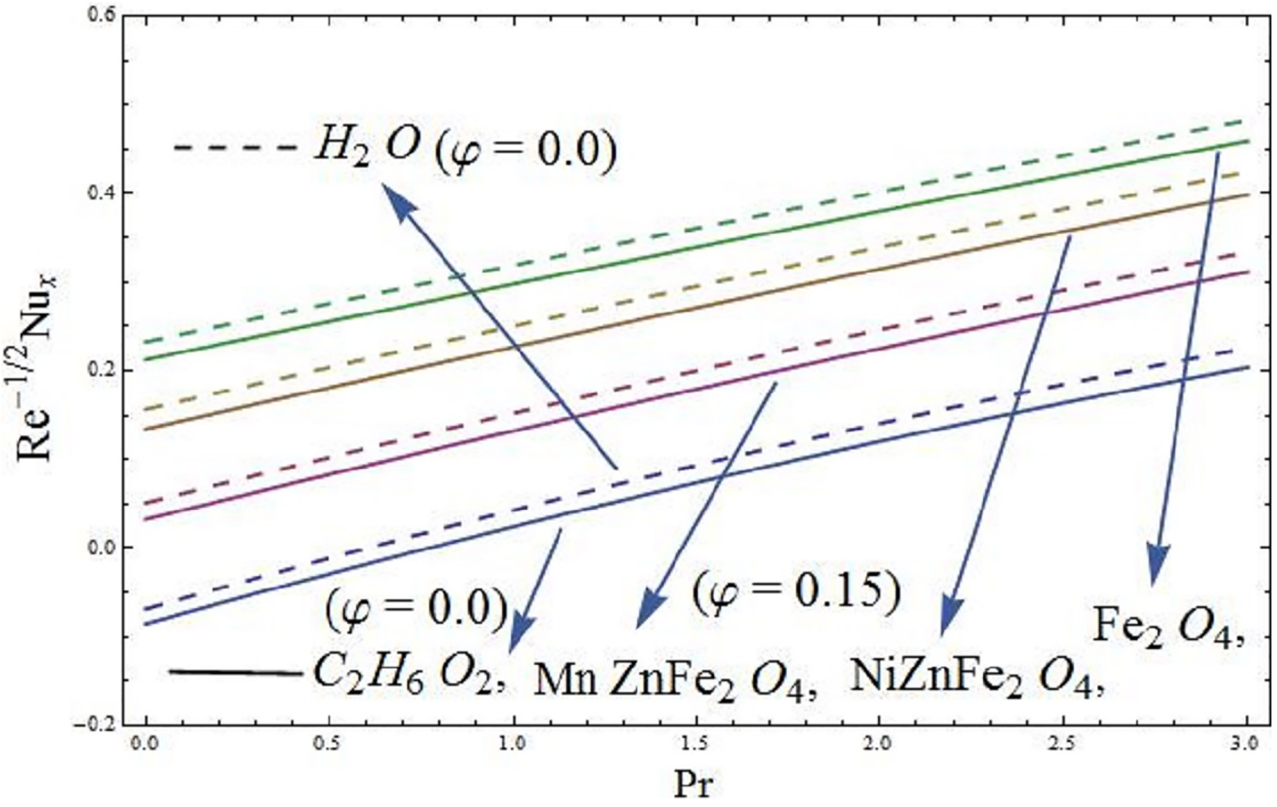

Fig 15. Heat transfer rate versus parameter Pr (Prandtl number).

https://doi.org/10.1371/journal.pone.0188460.g015

transfer rate is observed in presence of water based ferrite nanoparticles, instead, from Fig 15, it is evident that an increase in heat transfer rate is depicted for the respective ferromagnetic nanofluids. The values assigned to remaining parameters are $\lambda = 0.01$, $\lambda_1 = 0.3$, $\beta = 1.2$, $P_m = 0.5$, Pr = 6.96, and $\gamma = 0.1$.

Concluding remarks. The purpose of the article exhibit theoretically the practicability of the concept of ferromagnetic nanofluids with Fe_2O_4 (magnetite ferrite), $NiZnFe_2O_4$ (Nickel zinc ferrite), and $MnZnFe_2O_4$ (manganese zinc ferrite) as ferrites nanoparticles and H_2O (water) and $C_2H_6O_2$ (ethylene glycol) as base fluid. The heat transport phenomenon is depicted in the resulting ferromagnetic nanofluids. The boundary value problem is solved numerically and analytically with the help of BVPh2—mid point method and optimal homotopy analysis method respectively. The main points of the analysis are:

- An increase in φ (solid volume fraction of nanofluid) results in the reduction of axial velocity and enhances the temperature field.
- The existence of parameters P_m (Porosity) in the presence of Fe_2O_4 (magnetite ferrite), $NiZnFe_2O_4$ (Nickel zinc ferrite) and $MnZnFe_2O_4$ (manganese zinc ferrite) nanoparticles in a viscous carrier ferromagnetic nanofluid slow down the axial velocity.
- Axial velocity reduces and the temperature field enhances fastly for increasing values of β (ferromagnetic interaction) when magnetic dipole is present.
- The axial velocity and relative nano boundary layer of the ferromagnetic $NiZnFe_2O_4$—$C_2H_6O_2$, $NiZnFe_2O_4$—H_2O, $MnZnFe_2O_4$—$C_2H_6O_2$, $MnZnFe_2O_4$—H_2O, Fe_2O_4—

$C_2H_6O_2$, and Fe_2O_4—H_2O nanofluids are decreasing functions of λ_1 (conjugate parameter) and increasing function of temperature profile.

- Prandtl number results in the rapid depletion of the temperature field while enhancement in axial velocity in presence of magnetic dipole.
- The wall shear stress of the ferromagnetic $NiZnFe_2O_4$—$C_2H_6O_2$, $NiZnFe_2O_4$—H_2O, $MnZnFe_2O_4$—$C_2H_6O_2$, $MnZnFe_2O_4$—H_2O, Fe_2O_4—$C_2H_6O_2$, and Fe_2O_4—H_2O nanofluids enhances with parameters β (ferromagnetic interaction) and P_m (porosity).
- The fast reduction in heat transfer rate is observed in presence of magnetic dipole.

Future work. The present study can be investigated by incorporating convective boundary conditions, Newtonian heating, Darcy and non-Darcy porous media, Cattaneo-Christove heat and mass fluxes, variable thermal conductivity, variable mass diffusivity, Corban nanotubes etc. The features of ferrite nanoparticles can be disclosed in viscous fluids with various geometries. It will be considered in the near future with different kinds of fluid models. It is hoped that present study serves as a stimulus for drug delivery in biomedical processes.

Author Contributions

Conceptualization: Noor Muhammad.

Formal analysis: Noor Muhammad, Sohail Nadeem.

Funding acquisition: M. T. Mustafa.

Investigation: Noor Muhammad, Sohail Nadeem.

Methodology: M. T. Mustafa.

Project administration: M. T. Mustafa.

Resources: Sohail Nadeem, M. T. Mustafa.

Visualization: Noor Muhammad.

Writing – original draft: Noor Muhammad.

Writing – review & editing: Noor Muhammad, Sohail Nadeem.

References

1. Eastman JA, Choi SU, Li S, Yu W, and Thompson LJ. Anomalously increased effective thermal conductivities of ethylene glycol-based nanofluids containing copper nanoparticles. Appl Phys Lett. 2001 Feb; 78(6):718–720. https://doi.org/10.1063/1.1341218
2. Khan AU, Nadeem S, and Hussain ST. Phase flow study of MHD nanofluid with slip effects on oscillatory oblique stagnation point flow in view of inclined magnetic field. J Mol Liq. 2016 Dec; 224:1210–1219. https://doi.org/10.1016/j.molliq.2016.10.102
3. Afrand M, Toghraie D, and Ruhani B. Effects of temperature and nanoparticles concentration on rheological behavior of Fe_2O_4-Ag/EG hybrid nanofluid, an experimental study. Exp Therm Fluid Sci. 2016 Oct; 77: 38–44. https://doi.org/10.1016/j.expthermflusci.2016.04.007
4. Ahmed A and Nadeem S. Shape effect of Cu-nanoparticles in unsteady flow through curved artery with catheterized stenosis. Results Phys. 2017 Dec; 7:677–689. https://doi.org/10.1016/j.rinp.2017.01.015
5. Nadeem S and Ijaz S. Theoretical analysis of metallic nanoparticles on blood flow through stenosed artery with permeable walls. Phys Lett A. 2015 Mar; 379(6):542–554. https://doi.org/10.1016/j.physleta.2014.12.013

6. Mehmood R, Nadeem S, Saleem S, and Akbar NS. Flow and heat transfer analysis of Jeffery nanofluid impinging obliquely over a stretched plate. J Taiwan Inst Chem E. 2017 May; 74: 49–58. https://doi.org/10.1016/j.jtice.2017.02.001
7. Gireesha BJ, Mahanthesh B, and Gorla RS. Suspended particle effect on nanofluid boundary layer flow past a stretching surface. JON. 2014 Sep; 3(3):267–277.
8. Ahmed A and Nadeem S. The study of (Cu, TiO_2, Al_2O_3) nanoparticles as antimicrobials of blood flow through diseased arteries. J Mol Liq. 2016 Apr; 216:615–623. https://doi.org/10.1016/j.molliq.2016.01.059
9. Rashid I, Haq RU, and Al-Mdallal QM. Aligned magnetic field effects on water based metallic nanoparticles over a stretching sheet with PST and thermal radiation effects. Physica E Low Dimens Syst Nanostruct. 2017 May; 89:33–42. https://doi.org/10.1016/j.physe.2017.01.029
10. Sadaf H and Nadeem S. Analysis of combined convective and viscous dissipation effects for peristaltic flow of rabinowitsch fluid model. J Bionic Eng. 2017 Jan; 14(1):182–190. https://doi.org/10.1016/S1672-6529(16)60389-X
11. Choi SU. Enhancing thermal conductivity of fluids with nanoparticles. *ASME-Publications-Fed*. (1995) Jan; 231:99–106.
12. Muhammad N and Nadeem S. Ferrite nanoparticles Ni-$ZnFe_2O_4$, Mn-$ZnFe_2O_4$ and Fe_2O_4 in the flow of ferromagnetic nanofluid. Eur Phys J Plus. 2017 Sep; 132(9):377. https://doi.org/10.1140/epjp/i2017-11650-2
13. Javidi M, et al. Cylindrical agar gel with fluid flow subjected to an alternating magnetic field during hyperthermia. Int J Hyperthermia. 2015 Jan; 31(1):33–39. https://doi.org/10.3109/02656736.2014.988661 PMID: 25523967
14. Voit W, Kim DK, Zapka W, Muhammed M, and Rao KV. Magnetic behavior of coated superparamagnetic iron oxide nanoparticles in ferrofluids. Mater Res Soc Symp Proc. 2001 Jan; 676:Y7.8. https://doi.org/10.1557/PROC-676-Y7.8
15. Rosensweig RE. Magnetic fluids. Annu Rev Fluid Mech. 1987 Jan; 19(1):437–463. https://doi.org/10.1146/annurev.fl.19.010187.002253
16. Eringen AC and Maugin GA. Electrodynamics of continua II: fluids and complex media. NewYork, Springer 1990.
17. Bailey RL. Lesser known applications of ferrofluids. J Magn Magn Mater. 1983 Nov; 39(1–2):178–182. https://doi.org/10.1016/0304-8853(83)90428-6
18. Mee CD. The mechanism of colloid agglomeration in the formation of Bitter patterns. Proc Phys Soc. 1950 Aug; 63(8):922. https://doi.org/10.1088/0370-1298/63/8/122
19. Neuringer JL. Some viscous flows of a saturated ferrofluid under the combined influence of thermal and magnetic field gradients. Int J Non Linear Mech. 1966 Oct; 1(2):123–137. https://doi.org/10.1016/0020-7462(66)90025-4
20. Nadeem S, Raishad I, Muhammad N, and Mustafa MT. Mathematical analysis of ferromagnetic fluid embedded in a porous medium. Results Phys. 2017 Jan; 7:2361–2368. https://doi.org/10.1016/j.rinp.2017.06.007
21. Andersson HI and Valnes OA. Flow of a heated ferrofluid over a stretching sheet in the presence of a magnetic dipole. Acta Mech. 1998 Mar; 128(1):39–47. https://doi.org/10.1007/BF01463158
22. Zeeshan A, and Majeed A. Heat transfer analysis of Jeffery fluid flow over a stretching sheet with suction/injection and magnetic dipole effect. AEJ. 2016 Sep; 55(3):2171–2181.
23. Majeed A, Zeeshan A, and Ellahi R. Unsteady ferromagnetic liquid flow and heat transfer analysis over a stretching sheet with the effect of dipole and prescribed heat flux. J Mol Liq. 2016 Nov; 223:528–533. https://doi.org/10.1016/j.molliq.2016.07.145
24. Nadeem S, Ahmad S, Mustafa MT, and Muhammad N. Chemically reactive species in the flow of a Maxwell fluid. Results Phys. 2017 Jan; 7: 2607–2613. https://doi.org/10.1016/j.rinp.2017.06.017
25. Nadeem S and Muhammad N. Impact of stratification and Cattaneo-Christov heat flux in the flow saturated with porous medium. J Mol Liq. 2016 Dec; 224:423–430. https://doi.org/10.1016/j.molliq.2016.10.006
26. Muhammad N, Nadeem S, and Haq RU. Heat transport phenomenon in the ferromagnetic fluid over a stretching sheet with thermal stratification. Results Phys. 2017 Dec; 7:854–861. https://doi.org/10.1016/j.rinp.2016.12.027
27. Muhammad N, Nadeem S, and Mustafa MT. Squeezed flow of a nanofluid with Cattaneo—Christov heat and mass fluxes. Results Phys. 2017 Dec; 7:862–869. https://doi.org/10.1016/j.rinp.2016.12.028

28. Nadeem S, Ahmad S, and Muhammad N. Cattaneo-Christov flux in the flow of a viscoelastic fluid in presence of Newtonian heating. J Mol Liq. 2017 Jul; 237: 180–184. https://doi.org/10.1016/j.molliq.2017.04.080

29. Hayat T, Khan MI, Farooq M, Alsaedi A, Waqas M, and Yasmeen T. Impact of Cattaneo—Christov heat flux model in flow of variable thermal conductivity fluid over a variable thicked surface. Int J Heat Mass Transf. 2016 Aug; 220:702–710. https://doi.org/10.1016/j.ijheatmasstransfer.2016.04.016

30. Hayat T, Khan MI, Farooq M, Yasmeen T, and Alsaedi A. Stagnation point flow with Cattaneo-Christov heat flux and homogeneous-heterogeneous reactions. J Mol Liq. 2016 Aug; 220:49–55.

31. Farooq M, Khan MI, Waqas M, Hayat T, Alsaedi A, and Khan MI. MHD stagnation point flow of visco-elastic nanofluid with non-linear radiation effects. J Mol Liq. 2016 Sep; 221:1097–1103. https://doi.org/10.1016/j.molliq.2016.06.077

32. Salahuddin T, Khan I, Malik MY, Khan M, Hussain A, and Awais M. Internal friction between fluid particles of MHD tangent hyperbolic fluid with heat generation: Using coefficients improved by Cash and Karp. Eur Phys J Plus. 2017 May; 132(5):1–10. https://doi.org/10.1140/epjp/i2017-11477-9

33. Xu X and Chen S. Cattaneo—Christov heat flux model for heat transfer of Marangoni boundary layer flow in a copper—water nanofluid. Heat Tran Asian Res. 2017 Dec; 46(8):1281–1293. https://doi.org/10.1002/htj.21273

34. Waqas M, Khan MI, Hayat T, Alsaedi A, and Khan MI. On Cattaneo—Christov double diffusion impact for temperature-dependent conductivity of Powell—Eyring liquid. Chinese J Phys. 2017 Jun; 55 (3):729–737. https://doi.org/10.1016/j.cjph.2017.02.003

35. Hayat T, Zubair M, Waqas M, Alsaedi A, and Ayub M. On stratified variable thermal conductivity stretched flow of Walter-B material subject to non-Fourier flux theory. Neural Comput Appl. 2017 May:1–7.

36. Liao S. Beyond perturbation: Introduction to homotopy analysis method, Chapmanand Hall, CRC Press, Boca Raton (2003).

37. Liao S. Homotopy analysis method in non-linear differential equations. Springer and Higher Education Press, Heidelberg (2012).

38. Rashidi MM, Ganesh NV, Hakeem AA, Ganga B, and Lorenzini G. Influences of an effective Prandtl number model on nano boundary layer flow of γ Al_2O_3-H_2O and γ Al_2O_3-$C_2H_6O_2$ over a vertical stretching sheet. Int J Heat Mass Transf. 2016 Jul; 98:616–623. https://doi.org/10.1016/j.ijheatmasstransfer.2016.03.006